A multi-chemistry modelling framework to enable flexible and reproducible water quality simulations in existing hydro-models: 2. The OpenWQ-SUMMA and OpenWQ-CRHM model implementations and testing

Diogo Costa[1,2], Kyle Klenk[1], Wouter Knoben[1], Andrew Ireson[1], Raymond J. Spiteri[1], Martyn Clark[1]

[1]Mediterranean Institute for Agriculture, Environment and Development & Global Change and Sustainability Institute, Department of Geosciences, Universidade de Évora, Pólo da Mitra, Ap. 94, 7006-554 Évora, Portugal
[2]University of Saskatchewan, 105 Administration Pl, Saskatoon, SK S7N 5A2, Canada

Abstract

This work advances the cross-model deployment of ecological and biogeochemical simulation capabilities in existing process-based hydro-modeling tools, which we term "Open Water Quality" (OpenWQ). The companion paper details aspects of the OpenWQ architecture that enables its plug-in type incorporation into existing models, along with its innovative aspects that enable biogeochemistry lab-like capabilities. OpenWQ's innovative aspects allow modelers to define the pollution problem(s) of interest, the appropriate complexity of the biogeochemistry routines, test different modeling hypotheses, and deploy them across different hydro-models. In this second paper, we implemented the coupling recipe described in the first paper to integrate OpenWQ into two hydro-models, SUMMA and CRHM. Here we explain how the implemented coupling interface between the two models provides water quality simulation capacities in the host hydro-models but, more importantly, establishes a direct and permanent link for the transfer of innovation between the modeling communities. Example applications of different pollution studies enabled by our coupling recipe are also provided to address some of these fundamental water quality modeling challenges.

1 Introduction

Climate change is expected to affect many hydro-biogeochemical processes along the land-river-lake continuum (Costa et al., 2022). However, the specific local impacts of climate change on hydrology and water quality will vary regionally and seasonally. On the one hand, extreme winter river flows arising from increased extreme precipitation events are expected to occur with greater frequency worldwide (Alexander et al., 2020; Field & Barros, 2014; Luo et al., 2020; Onishi et al., 2020; "Effects of lake water level fluctuation due to drought and extreme winter precipitation on mixing and water quality of an alpine lake, Case Study: Lake Arrowhead, California", 2020; Shi et al., 2011; Suddick et al., 2013; H. Wilson et al., 2019; Yang et al., 2019; Zheng et al., 2020). On the other hand, summer river flows are projected to decrease across many regions around the world, including North America (Rood et al., 2008), China (Shi et al., 2011; Ervinia et al., 2020; Zheng et al., 2020), and western Europe (Charlton et al., 2018; Raimonet et al., 2018). In arid climates, the flow reduction is predicted to be particularly strong (Jarsjö et al., 2017; Shi et al., 2011; Y. Wu et al., 2012; Ye & Grimm, 2013; Bussi et al., 2021), reducing dilution of pollution point sources, including wastewater outlets (Bussi et al., 2017; Charlton et al., 2018; Raimonet et al., 2018; Ockenden et al., 2016; Whitehead et al., 2009).

The increase in climate variability is projected to lead to an overall increase in precipitation and snowmelt runoff, which, combined with changes in intensified cropping patterns, is anticipated to lead to greater freshwater nutrient pollution in temperate regions of North America, Europe and Japan (Alexander et al., 2020; Jeppesen et al., 2011; Onishi et al., 2020; H. F. Wilson et al., 2019). Increased nutrient uptake rates from terrestrial plants due to climate change are not expected to facilitate the increase in nutrient runoff losses (Luo et al., 2020; Sperotto et al., 2019; Suddick et al., 2013; Zheng et al., 2020). Erosivity from agricultural and urban nonpoint sources is also projected to increase with more intense runoff events because of their greater capacity to mobilize particulate and soluble N and P (El-Khoury et al., 2015; Ockenden et al., 2016, 2017; J. Wu & Malmström, 2015; Crossman et al., 2014).

Understanding the key factors controlling the fate of pollution in aquatic ecosystems is challenging because it requires capturing multiple climate, hydrological, and biogeochemical patterns across different spatial scales in models (Costa et al., 2022). Whilst there have been numerous modelling advances over the last decade, process representation, model intercomparability, model configuration (input data), and model validation remain key challenges in water quality. Another considerable difficulty with the application of water quality models is the often-limited monitoring data available for validation, which can compromise the confidence of scientists and decision-makers in their simulation results.

This two-part paper presents a methodology termed "OpenWQ" that tackles some of these fundamental modeling challenges by streamlining the transfer of knowledge, technology, and innovation between the different scientific and modeling communities related to water quality. Some of these scientific and modelling communities include biogeochemistry, soil science, hydrology, hydrodynamics, and hydrogeology. This work aims to provide a concrete, transformative framework for enhancing collaborative efforts and co-creation that can benefit the entire environmental and ecological research and management community. Our intent for the first paper was to advance OpenWQ's concept as a coupler and introduce its customizable biogeochemistry modeling framework. This customizable framework enables the cross-model deployment of eco-lab water quality modeling capabilities. This second paper builds on the motivation for OpenWQ introduced in the first paper and outlines the initial implementation of OpenWQ as a modeling system. The goals of this second paper are to

1. Demonstrate how OpenWQ has been integrated into two hydro-models using the coupling procedures laid out in the first paper. The hydro-models have been selected for their likewise flexible modeling frameworks, namely the Structure for Unifying Multiple Modeling Alternatives (SUMMA, Clark et al., 2015a,b) and the Cold Regions Hydrological Model and its water quality modules (CRHM/CRHM-WQ, J. W. Pomeroy et al., 2007; Costa et al., 2021).
2. Apply the multi-chemistry, eco-lab framework of OpenWQ incorporated with CRHM and SUMMA to examine a variety of common pollution problems.

2 Coupling to hydro-models

OpenWQ has been coupled to two hydro-models, SUMMA (Clark et al., 2015a,b) and CRHM/CRHM-WQ (J. Pomeroy et al., 2022; Costa et al., 2021; J. W. Pomeroy et al., 2007). In companion paper 1 *(CITE_paper_1)*, we explain how OpenWQ has been designed as a flexible coupler to streamline its integration in existing hydro-models. A coupling recipe has been developed to lay out the steps involved in the coupling process, which includes linking four coupling functions. Here, in paper 2, we explain how this coupling recipe was deployed in two separate coupling efforts and used to examine different pollution problems.

SUMMA SUMMA is written in Fortran, while OpenWQ is written in C++. Thus, it was necessary to create wrapper functions that allow for the interaction between a Fortran driver program and a C++ coupled program at runtime. Because it is OpenWQ that is integrated into SUMMA, the coupled model was constructed in a manner to allow SUMMA to manage the simulation timesteps. For this, we used the standard intrinsic Fortran module *iso_c_binding* that defines constants, types, and procedures for C interoperability. The *iso_c_binding* module is part of the language standard and makes the interface between Fortran and C standard and portable. Essentially, Fortran-to-C wrapper functions were created to allow SUMMA to interface with OpenWQ and, from the point of view of SUMMA, OpenWQ is an object to which it held a pointer upon initialization of OpenWQ. The wrapper functions allowed SUMMA to interface with OpenWQ's coupler functions as if they were method calls. Fortran-to-C wrapper functions were constructed for creating a reference to a OpenWQ along with each of the four OpenWQ C++ coupler functions (*openwq::decl*, *openwq::run_time_start*, *openwq::run_space*, and *openwq::run_time_end*; see Section 3.3.2 of the first paper *(CITE_paper_1)*.

CRHM Similar to OpenWQ, CRHM is written in C++. This avoids the need for wrapper interface functions as required in the SUMMA-OpenWQ coupling. CRHM already had a water quality module named CRHM-WQ that enables the simulation of the nitrogen (N) and phosphorous (P) cycles (Costa et al., 2021). Thus, CHRM already contains a solute transport simulation routine that moves contaminants through the hydrological cycle represented by the model. The native implementation of solute transport in CRHM-WQ is

limited to 6 chemical species related to the N and P cycles, namely nitrate (NO_3-N), ammonium (NH_4-N), dissolved organic nitrogen (DON), soluble reactive phosphorous (SRP), and particulate phosphorous (PP). Therefore, instead of coupling all four OpenWQ coupler functions to CRHM-WQ, we considered it more appropriate to use CRHM's native transport routine, which has already been tested, and adjust it for a more dynamic allocation of the number of chemical species when OpenWQ is activated, leaving OpenWQ's coupling routine for transport (*openwq::run_space*) out of the coupling process.

3 Case studies

3.1 Overal science questions

OpenWQ enables exploring multiple working hypotheses related to multi-chemistry biogeochemical cycling in different seasons, climate zones, and landscapes. The work aims to respond to critical challenges with water quality modeling as an interdisciplinary science, which have been highlighted in the companion paper *(CITE_paper_1)*. The specific modeling challenges addressed are to:

1. Identify appropriate biogeochemical frameworks: what are the key biogeochemical processes and chemical species that should be represented in models to capture the fate and controls of pollution in a way that is (1) adequate for the quantity and quality of the available data for model evaluation, (2) scientifically sound from a biogeochemical perspective, and (3) useful for the objectives of the study and helpful for decision making?
2. Differentiate controlling biogeochemical transformations across hydrological compartments (e.g., snow, groundwater, etc.): should biogeochemical processes be differentiated across hydrological compartments and regions, e.g., although the processes involved in the nitrogen cycle are the same regardless of the environment they occur in (e.g., nitrification, denitrification, assimilation, ammonification, nitrogen fixation), certain environmental conditions tend to favor particular processes (e.g., oxygen levels in groundwater tend to be low, leading to reduced nitrification rates because this is a process involving dissolved oxygen)?
3. Characterize model uncertainty: can we better understand the sources of uncertainty related to key modeling processes and methods used so that we can incrementally improve our models, increase predictability and model fidelity, and reduce parameter equifinality?

Some of these questions have also been raised by the hydrological community (Clark et al., 2015b; Reggiani et al., 1998; Beven, 2006; Renard et al., 2010; Wood et al., 2011), but the ones listed above extend to aspects specific to water quality modeling. The general concept of OpenWQ is to facilitate a test-improve workflow so that models can be flexibly and incrementally improved based on model results and inputs from different disciplines.

3.2 Model tests

The model was evaluated using a series of tests designed to expose the accuracy and robustness of the mathematical formulation and numerical solutions deployed for examining a variety of pollution problems. In recent years, it has been recognized that such basic tests are an essential step for proper model scrutiny, falsification, and acceptance (Clark et al., 2021a). In this study, we pioneer the extension of such important principles for water quality simulations where the spatiotemporal complexity and interplay of process generally often give rise to highly non-linear response patterns that are difficult to disentangle in real-world applications for proper model examination (Costa et al., 2022, 2020). The case study tests devised are representative of a variety of environmental pollution problems for

Table 1: Case study tests used to test OpenWQ and its coupling to SUMMA and CRHM

Transport Scheme	Designation	Description
No transport	1_noTrans_1species_1storder	Batch reactor involving 1 chemical species subject to first-order decay
	2_noTrans_1species_2ndorder	Batch reactor involving 1 chemical species subject to second-order decay
	3_noTrans_2species	Batch reactor involving 2 chemical species subject to first-order decay
	4_noTrans_3species	Batch reactor involving 3 chemical species subject to first-order decay
	5_noTrans_nitrogencycle	Batch reactor representing the nitrogen cycle
	6_noTrans_oxygenBODcycle	Batch reactor representing the dissolved oxygen cycle
Advection-Dispersion	7_trans_contS_PorMedia	Non-reactive transport of 1 chemical species in porous media subject to a continuous load
	8_trans_contS_PorMedia_1storder	Reactive (linear decay) transport of 1 chemical species in porous media subject to a continuous load
	9_trans_instS_PorMedia	Non-reactive transport of 1 chemical species in porous media subject to an instantaneous load
	10_trans_instS_PorMedia_1storder	Reactive (linear decay) transport of 1 chemical species in porous media subject to an instantaneous load

which analytical solutions have been either specially derived for this paper or taken from the literature.

We divide the tests into reactive and non-reactive. This is an important distinction because basic mass balance principles cannot be directly applied to reactive chemical constituents without proper consideration because they are subject to biogeochemical transformation in addition to physical transport. We prepared a total of ten tests, of which two are non-reactive and eight are reactive. Each of these tests has well-defined initial conditions, boundary conditions, sink and source terms, and is subject to specific biogeochemistry as described below. Based on these conditions, analytical solutions have been derived for comparison with the model results. In order to benefit the comparison of model results, the simulations are divided into two groups as shown in Table 1.

The case studies include six batch reactor-type tests, specifically two single-species tests and four multi-species tests. The single-species tests are the simplest and represent cases involving first- (Test 1) and second-order (Test 2) linear decay processes. The multi-species tests include (a) a two-species reaction network subject to linear decay (Test 3), (b) a three-species reaction network subject to linear decay (Test 4), and reaction networks to represent the (c) nitrogen (Test 5) and (d) dissolved oxygen (Test 6) cycles. The remaining four tests involve the transport of chemical constituents, specifically two non-reactive tests, one considering a continuous point source (Test 7), one considering an instantaneous points source (Test 8), and two reactive tests that are similar to the homologous non-reactive tests, but where chemical species undergo biogeochemical transformations (Tests 9 and 10, respectively).

3.3 Multi-chemistry lab set up

The case studies involve different pollution problems. In some cases, they are generic in the sense that they are representative of types of biogeochemical processes and could be applied to examine a variety of water quality problems. In other cases, the tests are more specific, focusing on environmental issues involving specific biogeochemical cycles, such as the nitrogen and phosphorous cycles. As mentioned in the first paper, the biogeochemistry calculation engine is flexible and easily extendible, supporting numerous forms of functional, logical, and vector processing semantics. It is enabled by the comprehensive C++ Mathematical Expression Toolkit Library (*ExprTk*) developed by Arash Partow (Partow, 1999). The implementation of ExprTk in OpenWQ is simple to use. It provides an efficient run-

time mathematical expression parser and evaluation engine that is ideal for testing different modeling hypotheses to inform incremental improvements to the model setup.

In order to perform the various pollution case study tests described in Table 1, a series of OpenWQ input files have been prepared. The biogeochemistry JSON files (see Section **??** of the first paper) are where the multi-chemistry lab simulations are characterized. We defined one biogeochemistry file per case study test, which we deployed in both SUMMA-OpenWQ and CRHM-OpenWQ coupled models. From paper 1, one of the transformative innovations of OpenWQ is the ability for cross-model deployment of eco-lab co-creation modeling capabilities using the same OpenWQ biogeochemistry JSON files. This allows the implementation of multiple hydro-biogeochemical modeling hypotheses by simply loading the desired JSON biogeochemistry file. The input files prepared for the different case study tests are publicly available on GitHub. They can be used as the basis for validation of any new coupling of OpenWQ to a hydro-model.

3.4 Deriving analytical solutions

In this section we provide details about the derivation of the analytical solutions used to verifying the performence of OpenWQ when coupled to SUMMA and CRHM. Each test is presented in a separate section, which starts with a diagram of relevent reaction network. The diagrams are then used to define the governing equations, which can be ordinary or partial differential equations. Finally, the derived analytical solution is presented. Details about the derivations is provided in the Appendix A-G.

3.4.1 Batch reactor: Single-species (Tests 1 and 2)

The single-species batch reactor tests involve (a) first-order and (b) second-order decay kinetics. Fig. 1 depicts the biogeochemical process.

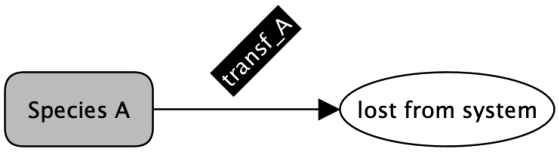

Figure 1: Single-species reaction network where transf_A is a first-order biogeochemical decay reaction.

The analytical solution of a single species subject to first-order decay can be obtained by integrating Eq. 24 with initial condition at time $t = 0$ to obtain Eq. 25. In turn, the analytical solution of a single species subject to second-order decay can be obtained by integrating Eq. 26 with initial condition at time $t = 0$ to obtain Eq. 27. See Appendix A for more details.

$$\frac{dc_A}{dt} = -kc_A \tag{1}$$

$$c_A(t) = c_A(0)e^{-kt} \tag{2}$$

$$\frac{dc_A}{dt} = -kc_A^2 \tag{3}$$

$$c_A(t) = \frac{1}{\frac{1}{c_A(0)} + kt} \tag{4}$$

3.4.2 Batch reactor: Two-species reaction network (Test 3)

The two-species reaction network with linear decay is represented schematically in Fig. 2.

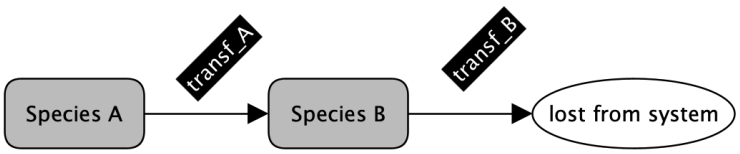

Figure 2: Two-species reaction network where transf_A and transf_B are first-order biogeochemical transformations.

Similar to the single-species case with first-order decay (Eq. 25), the fate of Species A in a two-species reaction network only depends on its own concentration and is given by Eq. 28.

$$c_A(t) = c_A(0)e^{-k_A t} \tag{5}$$

However, the fate of Species B depends on the time-evolution of concentrations of both Species A and B. This evolution can be expressed as:

$$\frac{dc_B}{dt} = k_A c_A - k_B c_B \tag{6}$$

The analytical solution of Eq. 29 with initial condition at time $t = 0$ can be obtained by using the integrating factor, $e^{k_B t}$. Details on this derivation are provided in the Appendix B. The solution is provided in Eq 38.

$$c_B(t) = c_B(0)e^{-k_B t} + \frac{k_A c_A(0)}{k_B - k_A}\left\{e^{-k_A t} - e^{-k_B t}\right\} \tag{7}$$

3.4.3 Batch reactor: Three-species reaction network (Test 4)

A three-species reaction network with linear decay is represented schematically in Fig. 2.

Concentrations of Species A and B are given by respectively Eqs. 28 and 38. The differential equation for the concentration of Species C can be written as:

$$\frac{dc_C}{dt} = k_B c_B - k_C c_C \tag{8}$$

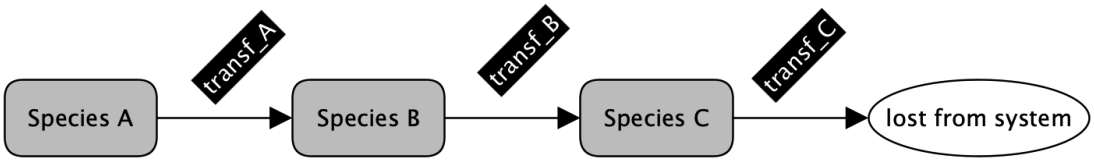

Figure 3: Three-species reaction network where transf_A, transf_B, and transf_C are first-order biogeochemical transformations.

The analytical solution Eq 40 can again be obtained by using the integrating factor $e^{k_C t}$. Details on this derivation are provided in the Appendix. The final solution is

$$c_C(t) = c_C(0)e^{-k_C t} - \frac{k_B}{k_B - k_C} c_B(0) \left(e^{-k_B t} - e^{-k_C t}\right) - \frac{k_B k_A}{(k_B - k_A)(k_C - k_A)} c_A(0) \left\{ \left(e^{-k_B t} - e^{-k_A t}\right) - \frac{e^{-k_C t}}{k_C - k_B} \right\}. \tag{9}$$

3.4.4 Batch reactor: Nitrogen cycle (Test 5)

The simulation of the nitrogen cycle is common in freshwater water quality studies because it allows for addressing issues with nutrient pollution and eutrophication. The nitrogen cycle simulated involves different nitrogen species (Fig. 4). The conceptual cycling framework used is similar to that used in catchment-scale models like HYPE Lindström et al. (2010), CRHM-WQ (Costa et al., 2021) models, SWAT (Arnold et al., 2012), and INCA ("A semi-distributed ntegrated itrogen model for multiple source assessment in tchments (INCA): Part I — model structure and process equations", 1998).

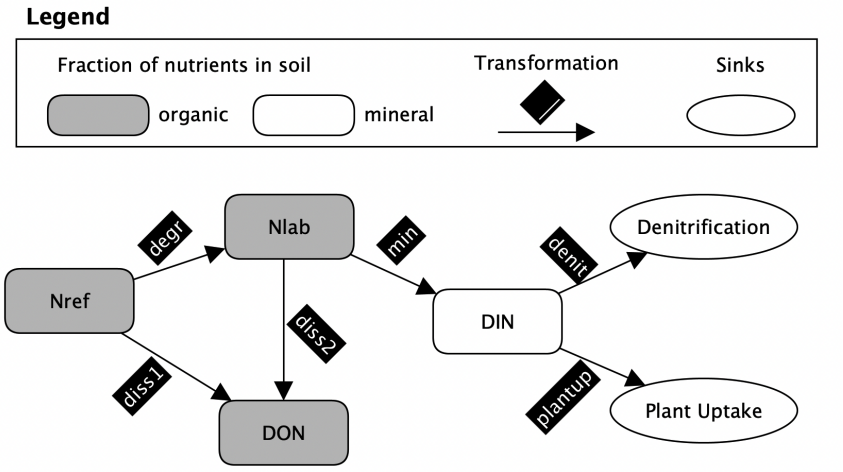

Figure 4: Nitrogen cycle as represented in several popular catchment-scale models. The nitrogen species $Nref$ refers to refractory nitrogen, $Nlab$ refers to labile nitrogen, DON refers to dissolved organic nitrogen, and DIN refers to dissolved innorganic nitrogen. The transformation $degr$ refers to degration; $diss1$ and $diss2$ refers to dissolution from $Nref$ and $Nlab$, respectively; min refers to mineralization; $denitr$ refers to denitrification; and $plantup$ refers to plant uptake.

The analytical solutions for the different nitrogen species can be obtained from Eq. 28, Eq. 38, or Eq. 47, depending on their positioning in the reaction chain:

Refractory N *(Nref)* Similar to Eq. 28, which for this specific processes and N species reads as

$$c_{Nref}(t) = c_{Nref}(0)e^{-(k_{degr}+k_{diss1})t} \tag{10}$$

Labile N *(Nref)* Similar to Eq. 38, which for this specific processes and N species reads as

$$\begin{aligned} c_{Nlab}(t) = c_{Nlab}(0)e^{-(k_{min}+k_{diss2})t} \\ + \frac{k_{degr}c_{Nref}(0)}{k_{min}+k_{diss2}-k_{degr}}\left\{e^{-k_{degr}t} - e^{-(k_{min}+k_{diss2})t}\right\}. \end{aligned} \tag{11}$$

Dissolved Organic N *(DON)* The concentration of DON does not depend on itself, but rather on the evolution of the concentration of $Nref$ and $Nlab$. The differential equation can be written as

$$\frac{dc_{DON}}{dt} = k_{diss1}c_{Nref} + k_{diss2}c_{Nlab} \tag{12}$$

Due to similarities in the relative positioning of the chemical species in the reaction network, analytical solutions suitable for c_{Nref} and c_{Nlab} are given by Eqs. 28 and 38, respectively. The derivation of Eq. 50 is provided in Appendix D, and its solution reads

$$\begin{aligned} c_{DON}(t) = c_{DON}(0) + \frac{k_{diss1}c_{Nref}(t)}{k_{degr}+k_{diss1}} - \frac{k_{diss2}c_{Nlab}(0)}{k_{min}+k_{diss2}} \\ - \frac{k_{diss1}c_{Nref}(t)}{k_{degr}+k_{diss1}}e^{-(k_{degr}+k_{diss1})t} - \frac{k_{diss2}c_{Nlab}(0)}{k_{min}+k_{diss2}}e^{-(k_{min}+k_{diss2})t} \\ + \frac{k_{diss2}k_{degr}c_{Nref}(t)}{k_{min}+k_{diss2}-k_{degr}}\left\{\frac{e^{(k_{min}+k_{diss2})t}-1}{k_{min}+k_{diss2}} - \frac{e^{-k_{degr}t}}{k_{degr}-1}\right\}. \end{aligned} \tag{13}$$

Dissolved Inorganic N *(DIN)* The ordinary differential equation for DIN can be written as

$$\frac{dc_{DIN}}{dt} = k_{min}c_{Nlab} - (k_{denit}+k_{plantup})c_{DIN}. \tag{14}$$

The analytical form for the concentration of $c_{Nlab}(t)$ is given in Eq. 49 and can be substituted in Eq. 56 to initiate the derivation that is provided in the Appendix. The analytical solution to Eq. 56 reads

$$
\begin{aligned}
c_{DIN}(t)e^{\left[(k_{denit}+k_{plantup})t\right]} &= c_{DIN}(0) \\
+k_{min}c_{Nlab}(0)&\left\{\frac{e^{\left[(k_{denit}+k_{plantup}-k_{min}-k_{diss2})t\right]}-1}{k_{denit}+k_{plantup}-k_{min}-k_{diss2}}\right\} \\
+\frac{k_{min}k_{degr}c_{Nref}(0)}{k_{min}+k_{diss2}-k_{degr}}&\left\{\frac{e^{\left[(k_{denit}+k_{plantup}-k_{degr})t\right]}-1}{k_{denitr}+k_{plantup}-k_{degr}}\right. \\
&\left.-\frac{e^{\left[(k_{denit}+k_{plantup}-k_{min}-k_{diss2})t\right]}-1}{k_{denit}+k_{plantup}-k_{min}-k_{diss2}}\right\}
\end{aligned} \tag{15}
$$

3.4.5 Batch reactor: Dissolved oxygen cycle (Test 6)

Dissolved oxygen (DO) depletion in rivers and lakes is a common consequence of pollution. It typically occurs near discharge outlets of untreated wastewater and can lead to high levels of organic matter that, during decomposition by aerobic bacteria, causes a DO sag in the water column. For the purposes of DO dynamics, such organic matter is typically translated into units of biological oxygen demand (BOD). Fig. 5 depicts the processes involved, and the Streeter–Phelps equation (Streeter & Phelps, 1925) has long been used for such problems. It reads

$$\frac{dD}{dt} = k_1 L_t - k_2 D, \tag{16}$$

where D is the saturation deficit in g/m^3, which can be derived from the dissolved oxygen concentration at saturation minus the actual dissolved oxygen concentration ($D = DO_{sat} - DO$); k_1 is the deoxygenation rate, usually in d^{-1}; $L_t = L_a e^{-k_1 t}$; L_a is the initial oxygen demand of organic matter in the water, also called the ultimate BOD (BOD at time $t = \infty$); and k_2 is the reaeration rate, usually in d^{-1} . The unit of L_a is g/m^3; k_1; L_t is the oxygen demand remaining at time t, and t is the elapsed time, usually in days.

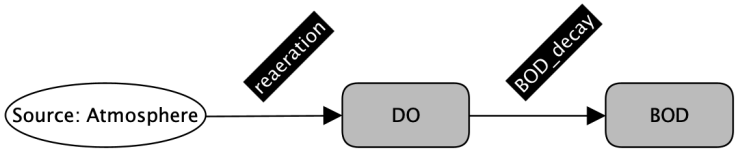

Figure 5: Representation of the transformations involved in the $BOD - DO$ cycle

The equation states that the total rate of change in oxygen deficit (D) is equal to the difference between the two rates of deoxygenation and reaeration at any time. See more details in Appendix E. The solution reads

$$D = \frac{k_1 L_a}{k_2 - k_1}\left\{e^{-k_1 t} - e^{-k_2 t}\right\} + D_a e^{-k_2 t}. \tag{17}$$

where D_a is the initial oxygen deficit $[g/m^3]$.

3.4.6 Reactive and non-reactive transport: Instantaneous point source (Tests 7 and 8)

These tests were only performed with SUMMA-OpenWQ because, as mentioned before, while OpenWQ's biogeochemical simulation modules have been integrated in both SUMMA-OpenWQ and CRHM-OpenWQ, OpenWQ's solute transport simulation modules were only

integrated in SUMMA-OpenWQ, but not in CRHM-OpenWQ, since CRHM has it's own solute transport routines (Costa et al., 2021). The general 1D diffusion-advection-reaction partial differential equation is given by

$$\frac{\partial c}{\partial t} = D_x \frac{\partial^2 c}{\partial x^2} - \nu \frac{\partial c}{\partial x} - \lambda c, \tag{18}$$

where c is the concentration of the tracer, t is time, D_x is the diffusion coefficient in the flow direction, x is the distance in the flow direction, ν is the flow velocity in the x-direction, and λ is a linear reaction term that can be set to zero for non-reactive tracers. Various analytical solutions for Eq. 18 have been derived and compiled by Wexler (1992) for different idealized scenarios.The modified equation for an instantaneous point source reads

$$\frac{\partial c}{\partial t} = D_x \frac{\partial^2 c}{\partial x^2} - \nu \frac{\partial c}{\partial x} - \lambda c + \frac{Q}{n} dt c_0 \delta\Big\{x - x_c\Big\}\delta\Big\{t - t'_c\Big\}, \tag{19}$$

where δ is the Dirac delta (impulse) function, x_c is the location of the instantaneous point source, t'_c is the time at which the instantaneous point source is activated, Q is the fluid injection rate, and n is the aquifer porosity. The analytical solution to Eq. 67 has been derived by Bear (1979) considering the following boundary conditions and initial conditions.

1. Boundary conditions (Neumann or second type):
   $c, \nabla c = 0, \quad x = \pm\infty$
2. Initial conditions:
   $c(x, t = 0) = 0, \quad -\infty < x < \infty.$

The analytical solution of Eq. 67 is given by

$$\begin{aligned} c(x) = \frac{c_0 Q}{4n\pi\gamma D_x} \exp\left[\frac{\nu(x - x_0)}{2D_x}\right] \\ \int_0^t \frac{1}{t} \exp\left[-\Big(\frac{\nu^2}{4D_x}\Big)\tau - \frac{(x - x_c)^2}{4D_x\tau}\right]. \end{aligned} \tag{20}$$

and can be used for solutes that are non-reactive (Test 7) or reactive (Test 8) by setting $\lambda = 0$ in Test 7.

The equation assumes that (1) the fluid has constant density and viscosity, (2) the solute may be subject to first-order chemical transformation, (3) the flow is uniform in the x-direction only, (4) the flow velocity is constant, and (5) the longitudinal diffusion coefficient (D_x) is constant. The solution has a mathematical singularity in the point source region (Abdelaziz et al., 2013) because it takes the form of the exponential integral when both $x - x_c$ approaches zero, hence becoming infinite at $\tau = 0$. However, according to Wexler (1989) the solution is still valid as long as $(x - x_c)^2$ is larger than ν^2, as it is the case in our tests.

3.4.7 Reactive and non-reactive transport: Continuous point source (Tests 9 and 10)

Similarly to Tests 7 and 8, the tests here have only been performed for SUMMA-OpenWQ due to the same reasons highlighted above in Section 3.4.6. The analytical solution for the transport of solutes with a continuous point source has been derived in Wexler (1992) after modification from Bear (1979) and Genuchten & Alves (1982).

Table 2: Model configuration for the different test cases

Transport Scheme	Designation	Reference	Biogeochemistry		Transport
			Initial Conditions	Reaction kinetics	
Batch Reactor	1_noTrans_1species_1storder	Fig. 1	Species A (c_0 = 10 mg/l)	k_{transf_A} = 0.01 $^1/_{day}$	NA
	2_noTrans_1species_2ndorder	Fig. 1	Species A (c_0 = 10 mg/l)	k_{transf_A} = 0.01$^1/_{day}$	NA
	3_noTrans_2species	Fig. 2	Species A (c_0 = 10 mg/l) Species B (c_0 = 0 mg/l)	k_{transf_A} = 0.03 $^1/_{day}$ k_{transf_B} = 0.01 $^1/_{day}$	NA
	4_noTrans_3species	Fig. 3	Species A (c_0 = 10 mg/l) Species B (c_0 = 0 mg/l) Species C (c_0 = 0 mg/l)	k_{transf_A} = 0.03 $^1/_{day}$ k_{transf_B} = 0.01 $^1/_{day}$ k_{transf_C} = 0.005 $^1/_{day}$	NA
	5_noTrans_nitrogencycle	Fig. 4	Nref (c_0 = 10 mg/l) Nlab (c_0 = 10 mg/l) DIN (c_0 = 5 mg/l) DON (c_0 = 2 mg/l)	k_{degrd} = 0.006 $^1/_{day}$ $k_{dissol-1}$ = 0.0002 $^1/_{day}$ $k_{dissol-2}$ = 0.0003 $^1/_{day}$ k_{miner} = 0.003 $^1/_{day}$ k_{denitr} = 0.001 $^1/_{day}$ $k_{plantup}$ = 0.001 $^1/_{day}$	NA
	6_noTrans_oxygenBODcycle	Fig. 5	BOD (c_0 = 10 mg/l) DO (c_0 = 12 mg/l)	$k_{BODdegrad}$ = 0.1 $^1/_{day}$ $k_{reaertion}$ = 0.5 $^1/_{day}$	NA
Advection-Dispersion	7_trans_contS_PorMedia	NA	Species A (c_0 = 0 mg/l)	NA	D_z = 0.0001 $^{m^2}/_s$
	8_trans_contS_PorMedia_1storder	Fig. 1	Species A (c_0 = 0 mg/l)	k_{transf_A} = 0.01 $^1/_{day}$	D_z = 0.0001 $^{m^2}/_s$
	9_trans_instS_PorMedia	NA	Species A (c_0 = 0 mg/l)	NA	D_z = 0.0001 $^{m^2}/_s$
	10_trans_instS_PorMedia_1storder	Fig. 1	Species A (c_0 = 0 mg/l)	k_{transf_A} = 0.01 $^1/_{day}$	D_z = 0.0001 $^{m^2}/_s$

$$c(x) = \frac{c_0}{2}\Bigg\{ \exp\left[\frac{x}{2D_x}(\nu - U)\right]\mathrm{erfc}\left[\frac{x - Ut}{2\sqrt{D_x t}}\right] + \exp\left[\frac{x}{2D_x}(\nu + U)\right]\mathrm{erfc}\left[\frac{x + Ut}{2\sqrt{D_x t}}\right]\Bigg\}, \tag{21}$$

where c_0 is the concentration of the continuous point source, $U = \sqrt{\nu^2 + 4\lambda D}$ and erfc is the complementary error function. Parameter λ is the first-order reaction rate used for Test 10, which can be set to zero for Test 9. See more details in Appendix G.

3.5 Model configuration and input files

The configuration of OpenWQ for the different test cases is summarized in Table 2. The analytical solutions described in Section 3.4 have been set up using the same initial and boundary conditions. The configuration of OpenWQ involves the characterization of biogeochemistry (initial conditions and reaction kinetics) and transport processes. The OpenWQ input files set up to translate the model configurations described in Table 2 are publicly available at `https://github.com/ue-hydro/synthetic_tests`. These input files can be used with any hydro-model coupled to OpenWQ and constitute an essential verification step in any new coupling project.

This public repository also contains the input files of the host hydro-models CRHM and SUMMA prepared for each model test, which have, in essence, been set up to provide no-flow conditions for Tests 1 to 6 (batch-reactor simulations) and steady-state conditions for Tests 7 to 10 (reactive and non-reactive transport simulations). Setting up proper flow conditions was a critical step to ensure the validity of the analytical solutions used to verify the numerical results. In the case of Tests 7 to 10 (transport simulations), which were only performed for SUMMA-OpenWQ as explained before, were based on the soil unsaturated flow test cases formulated by Celia et al. (1990), which have been set up in SUMMA as described in Clark et al. (2021b). The soil properties of these tests are described in Table 2 of that paper.

4 Results

The model results have been compared to the respective analytical solutions to verify the accuracy of OpenWQ in examining a variety of pollution problems. These tests contemplate

several biogeochemical processes that are often the object of study in environmental studies. The Nash–Sutcliffe efficiency (NSE) coefficient and the Root-Mean-Square Error (RMSE) were used to quantify the accuracy of the numerical results.

$$NSE = 1 - \frac{\sum(X_{obs} - X_{mod})^2}{\sum(X_{obs} - \mu_{obs})^2} \tag{22}$$

$$RMSE = \sqrt{\frac{\sum(X_{obs} - X_{mod})^2}{n}} \tag{23}$$

where X_{obs} and X_{mod} are the observed and simulated concentrations, μ_{obs} is the concentration average, and n is the number of observations. NSE values equal to one indicate a perfect match between observations and model results, and NSE values equal to zero indicate model predictions as accurate as the mean of all observations.

4.1 Batch reactor: Single-species (Tests 1 and 2)

The results of Tests 1 and 2 contemplate the general cases of single chemical species subject to first- or second-order decay as presented in Fig. 6. Such reaction types are commonly used in sequence or parallel to represent complex reaction networks.

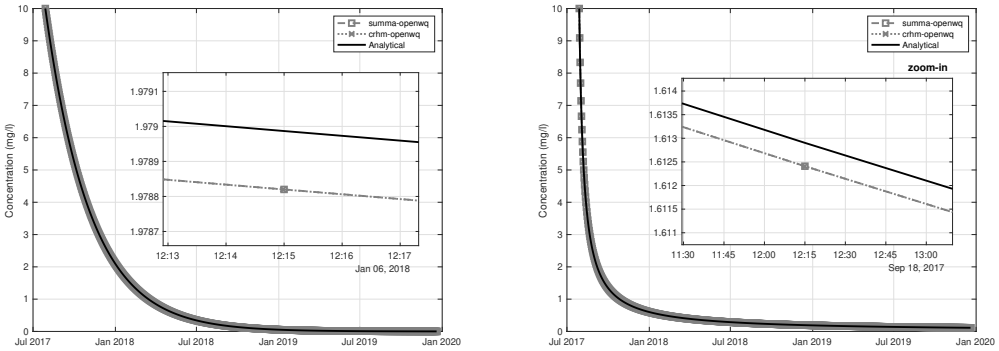

(a) Test 1 (1_noTrans_1species_1storder) (b) Test 2 (2_noTrans_1species_2ndtorder)

Figure 6: Comparison between model results and analytical solution for Tests 1 and 2

The results show good model predictability and reduced numerical dispersion. For Test 1, the Nash-Sutcliffe and RMSE values obtained for summa-openwq were respectively 0.999999998259312 and 8.804e-05 mg/l and for crhm-openwq were 0.999999998259309 and 8.804e-05 mg/l. For Test 2, the Nash-Sutcliffe and RMSE values obtained for summa-openwq were 0.999999900146240 and 3.0319e-04 mg/l, and for crhm-openwq were respectively 0.999999900145974 and 3.0319e-04 mg/l. The results obtained with summa-openwq and crhm-openwq are similar, which was expected since these tests deal only with biogeochemical transformations and nutrient transport, which is driven by the host-models, is not activated. The RMSE is one order of magnitude higher for Test 2, which was also anticipated given that the biogeochemical formulation in this test contains an exponent (i.e., power of two), which magnifies the propagation of round-off errors.

4.2 Batch reactor: Two-species reaction network (Test 3)

The results of Test 3 are presented in Fig. 7 and compared against analytical solutions. Two-species reaction networks are also common in water quality models and often integrated within comprehensive biogeochemical cycling representations.

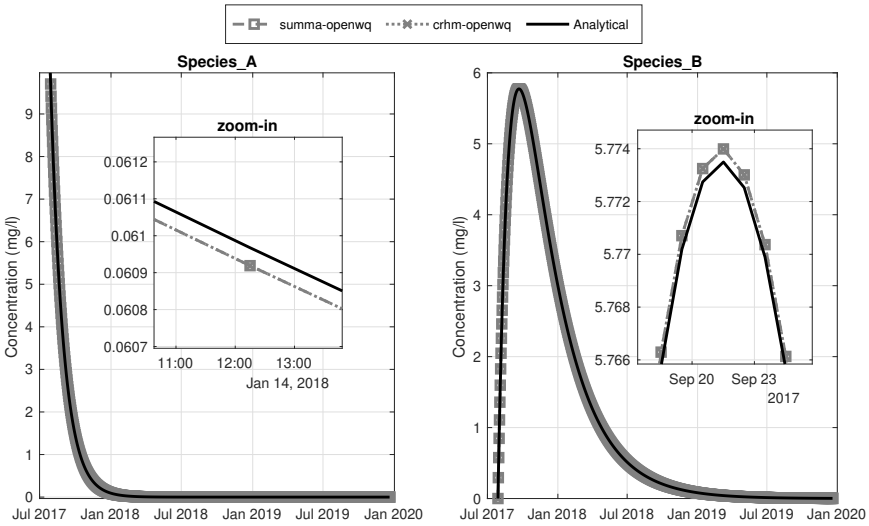

Figure 7: Comparison between model results and analytical solution for Test 3

The model shows good agreement with the analytical solution for Test 3, including the results for both Species A and B. For Species A, the Nash-Sutcliffe and RMSE values obtained for summa-openwq were 0.999999987172389 and 1.525e-04 mg/l, and for crhm-openwq were respectively 0.999999987172368 and 1.525e-04 mg/l. For Species B, the Nash-Sutcliffe and RMSE values obtained for summa-openwq were 0.999999989757722 and 1.747e-04 mg/l, and for crhm-openwq were respectively 0.999999989757706 and 1.747e-04 mg/l. The RMSE calculated for Species B is slightly higher than that calculated for Species A. This was anticipated since the reaction network sequence starts with Species A; thus, the effect of changes in the concentration of Species A will take one time step to travel to Species B. Reducing the length of the time step reduces the problem.

4.3 Batch reactor: Three-species reaction network (Test 4)

Fig. 8 shows the model results for Test 4, comparing the numerical solution with the corresponding analytical solution. This constitutes a more complex reaction chain that is often integrated into more complex biogeochemical cycling frameworks.

Similarly to the previous tests, the model demonstrates good accuracy and reduced numerical dispersion. For Species A, the Nash-Sutcliffe and RMSE values obtained for summa-openwq were respectively 0.999999987172389 and 1.524e-04 mg/l and for crhm-openwq were 0.999999987172368 and 1.524e-04 mg/l. For Species B, the Nash-Sutcliffe and RMSE values obtained for summa-openwq were respectively 0.999999989757722 and 1.747e-04 mg/l and for crhm-openwq were 0.999999989757706 and 1.747e-04 mg/l. For Species C, the Nash-Sutcliffe and RMSE values obtained for summa-openwq were respectively 0.999899420454185 and 1.560e-02 mg/l and for crhm-openwq were 0.999899420454600 and 1.560e-02 mg/l.

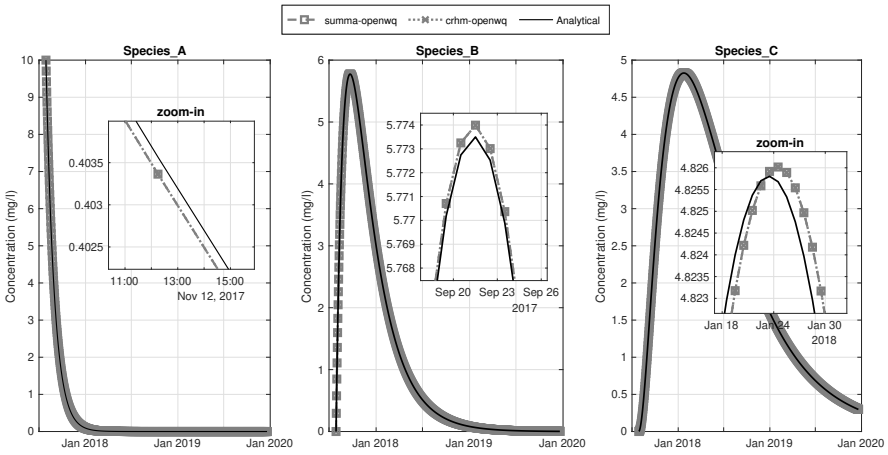

Figure 8: Comparison between model results and analytical solution for Test 4

A small phase shift can be noticed for Species C, which is also caused by the reaction network sequence issue mentioned in the previous test (Test 3). In OpenWQ, the hydro-models (CRHM and SUMMA) control the model time step. In these tests, the time step used was 15 minutes and was dictated by the data time intervals. The larger the time step is, the larger the shifts are expected to become since the computation of the reactions depends on the concentrations in the antecedent time step. So, in this case, a change in Species A has taken 30 min (2 times 15 minutes) to numerically travel to Species C, producing a slight phase shift. Reducing the length of the time step reduces the problem.

4.4 Batch reactor: Nitrogen cycle (Test 5)

The results of the nitrogen cycle simulation show good agreement with the numerical solution (Fig. 9). This is a reaction network involving four nitrogen species and it is commonly used in popular models such as HYPE, INCA, and SWAT.

The model shows good agreement with the analytical solution, reinforcing the confidence in OpenWQ's numerical solution and the implementation of the expression evaluator based on the comprehensive C++ Mathematical Expression Toolkit Library (*ExprTk*) developed by Arash Partow (Partow, 1999). For $Nref$, the Nash-Sutcliffe and RMSE values obtained for summa-openwq were respectively 0.999999999184531 and 6.927e-05 mg/l and for crhm-openwq were 0.999999999184529 and 6.927e-05 mg/l. For $Nlab$, the Nash-Sutcliffe and RMSE values obtained for summa-openwq were respectively 0.999136304357914 and 9.426e-02 mg/l and for crhm-openwq were 0.999136304357383 and 9.426e-02 mg/l. For DON, the Nash-Sutcliffe and RMSE values obtained for summa-openwq were respectively 0.999463220618209 and 1.3089e-02 mg/l and for crhm-openwq were 0.999463220618758 and 1.309e-02 mg/l. For DIN, the Nash-Sutcliffe and RMSE values obtained for summa-openwq were respectively 0.996669866632908 and 7.181e-02 mg/l and for crhm-openwq were 0.996669866633266 and 7.181e-02 mg/l. As in the previous reaction networks tested, the RMSE increases as the information travels through the network sequence: DIN ¿ $Nref$. This is caused by the same issue raised above related to the time of travel of information through the network sequence computation.

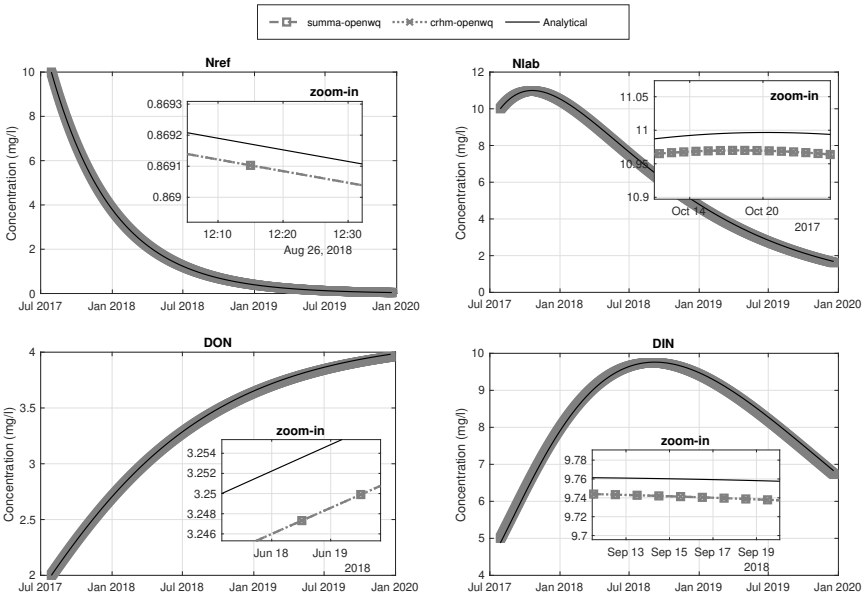

Figure 9: Comparison between model results and analytical solution for Tests 5

4.5 Batch reactor: Dissolved oxygen cycle (Test 6)

The simulation of the dissolved oxygen cycle is presented in Fig. 10 with two water quality variables (1) dissolved oxygen (DO) and (2) biological oxygen demand (BOD). This is also a common pollution problem simulated by water quality models to evaluate mitigation strategies for contamination caused by urban wastewater discharges in rivers and lakes.

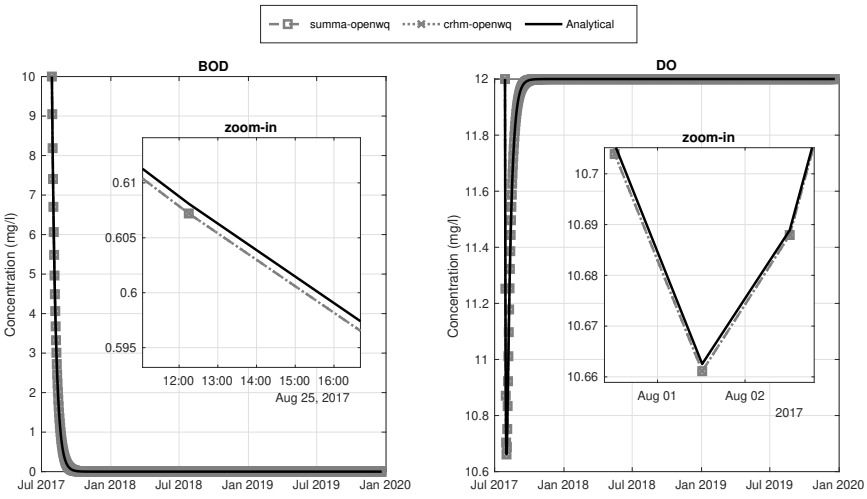

Figure 10: Comparison between model results and analytical solution for Tests 6

The model shows good agreement with observations, capturing the typical DO sag often observed near discharge outlets as predicted by the analytical solution. For DO, the Nash-Sutcliffe and RMSE values obtained for summa-openwq were respectively 0.999998916342720 and 1.416e-04 mg/l and for crhm-openwq were 0.999998916342720 and 1.416e-04 mg/l. For BOD, the Nash-Sutcliffe and RMSE values obtained for summa-openwq were respectively 0.999999874118595 and 2.783e-04 mg/l and for crhm-openwq were 0.999999874118595 and 2.783e-04 mg/l. As in the previous cases, the RMSE increases through the reaction network sequence, which is higher for BOD, despite that the Nash-Sutcliffe value remains very high for both species.

4.6 Reactive and non-reactive transport: Continuous point source (Tests 7 and 8)

Fig. 11 compares model results against analytical solutions for Tests 7 and 8, which represent non-reactive and reactive scenarios of transport of a continuous pollution source through porous media. The results show the traveling of solute through the soil profile driven by advection and dispersion processes. In the case of Test 8 in Fig 11b, there is an additional first-order biogeochemical reaction causing a linear decay in the concentrations. Each figure shows the computed concentrations, as well as the model internal derivatives that have been passed into the numerical solver to compute the concentration update. This is useful information to understand the key processes controlling the concentration of the solute as time progresses, as well as the relative contributions of transport and biogeochemistry.

Comparing Figs 11a and 11b, it becomes clear that the superposition of the different processes (e.g., biogeochemistry, physical transport) gives rise to a highly non-linear response that the model can capture accurately. For Test 7, the Nash-Sutcliffe and RMSE values obtained were respectively 0.9890 and 0.0747e-05 mg/l, and for Test 8 were respectively 0.9953 and 0.0392 mg/l. Results show that the Nash-Sutcliffe values remain high, but they are slightly lower when compared to the purely biogeochemical kinetic Tests 1-6. The opposite is observed for RMSE, where values have slightly increased. This minor deterioration of the numerical results with the activation of the transport routines was expected and it remains within acceptable values. This is caused by the initial conditions required to translate in the host-model to represent those set up in the analytical solutions, as well as the velocity fields computed by the host model and associated numerical dispersion in both OpenWQ and the host-model.

4.7 Reactive and non-reactive transport: Instantaneous point source (Tests 9 and 10)

The non-reactive and reactive tests for an instantaneous point source problem are shown in respectively Figs. 12a and 12b. Like in the previous case there is an additional first-order biogeochemical reaction causing a linear decay in the concentrations of Test 10 in Fig 12b.

For Test 9, the Nash-Sutcliffe and RMSE values obtained were respectively 0.9535 and 4.614e-05 mg/l, and for Test 10 were respectively 0.9521 and 1.409e-05 mg/l. The effect of biogeochemistry in the resulting concentrations can be also clearly observed in the upper-middle panel of Fig. 12a as compared to the upper-middle panel of Fig. 12b. Similarly to the previous cases of Tests 7 and 8, results show that the Nash-Sutcliffe values remain high, but they are slightly lower when compared to the purely biogeochemical kinetic Tests 1-6.

5 Conclusions

This two-part paper describes and applies a methodology for incorporating and cross-model deploying multi-biogeochemistry and ecological simulations in existing process-based hydro-modeling tools, the OpenWQ framework. OpenWQ was developed based on the motivation that (1) hydrology has a strong impact on the fate of pollution in the environ-

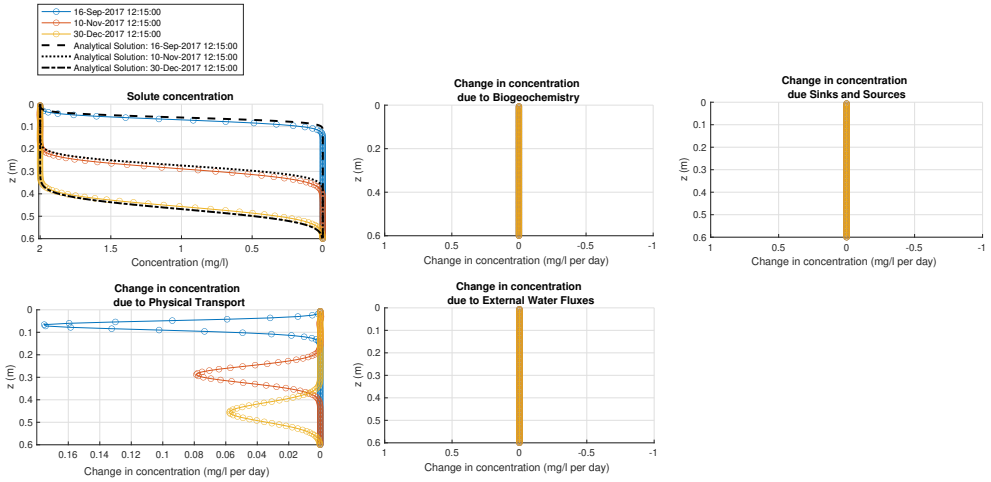

(a) Test 7

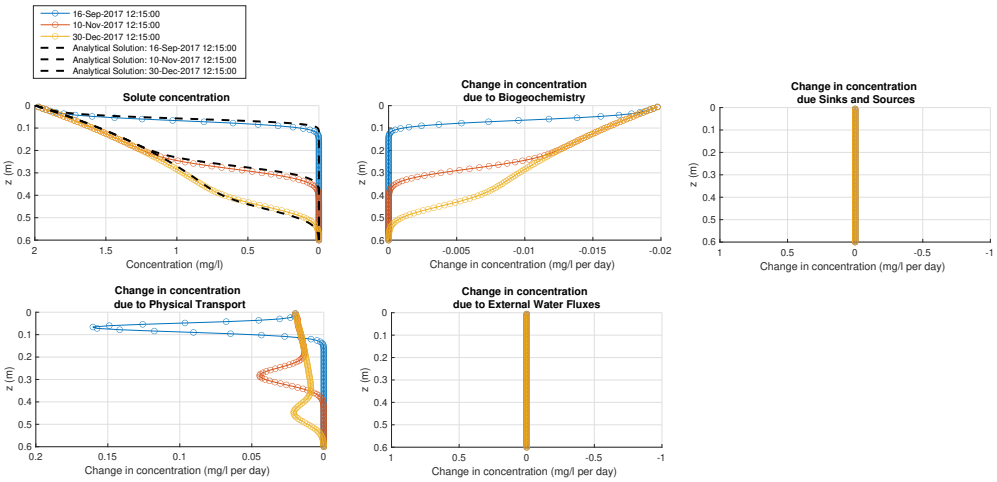

(b) Test 8

Figure 11: Comparison between model results and analytical solution for Tests 7 and 8

ment and (2) more should be done to streamline collaboration between the hydrological and biogeochemical communities. The first paper describes OpenWQ's concept as a coupler and customizable biogeochemistry modeling framework to allow cross-model deployment of eco-lab and co-creation modeling capabilities, providing a transformative direction for innovation in water quality modeling. This approach aims to address the inherent challenge of water quality modeling of being at the intersection between several fields, including biogeochemistry, soil science, hydrology, hydrodynamics, and hydrogeology.

This second paper describes the integration of OpenWQ into two hydro-models, SUMMA and CRHM, illustrating how coupling interfaces between the two models have not only enabled water quality simulation capacities in the host hydro-models but, even more importantly, enabled establishing a direct and permanent link for transfer of knowledge, innovation, and technology between modeling communities. Example applications of

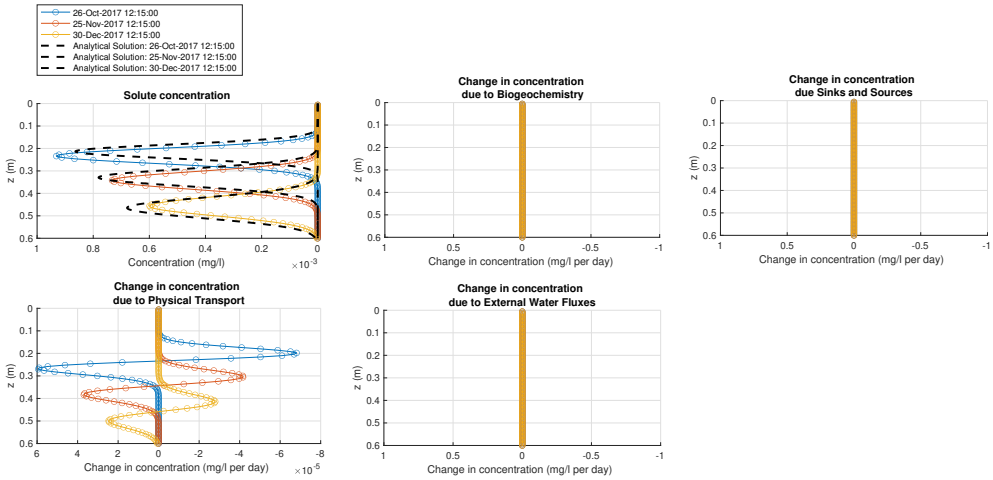

(a) Test 9

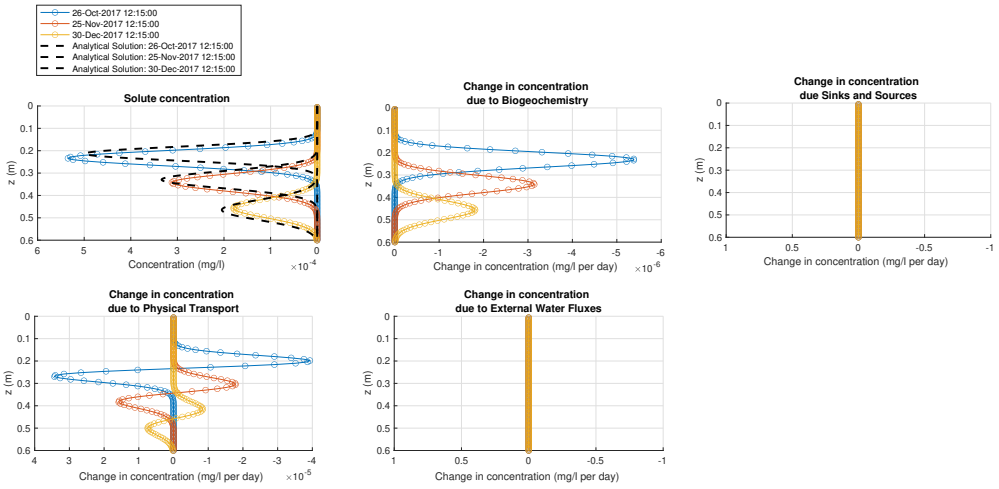

(b) Test 10

Figure 12: Comparison between model results and analytical solution for Tests 9 and 10

pollution studies enabled by the coupling of the tools are provided to begin to address some of these fundamental modeling challenges.

The key points of this paper are as follows:

1. The coupling of OpenWQ to CRHM and SUMMA illustrates how the coupling recipe presented in Paper 1 can be deployed to link the model to existing hydro-models even if displaying drastically different modeling structures. The coupling steps, coupling functions, and wrapper interface functions have been designed to optimize the coupling process. It was also demonstrated that new updates to OpenWQ can be integrated into the coupled models without requiring changes in the coupler functions. This provides a permanent, concrete link between the hydrological and biogeochemical research communities, where innovations on either side can be readily

integrated through the coupler into a unified modeling framework.

2. The model development and applications presented illustrate how OpenWQ's flexible multi-chemistry lab capabilities enable addressing a variety of environmental and pollution problems. In Paper 1, we described how such model flexibility has been materialized. In this paper, we deployed the model to illustrate how it can be used to look at the nitrogen cycle and eutrophication problems, BOD-DO and DO sag issues, and other environmental problems involving reaction networks run in parallel or sequence.

3. The model applications presented aim to illustrate how biogeochemical modeling frameworks can be readily deployed across different hydro-models using the same input files. It has been shown how this can be extremely helpful in removing barriers in the selection of the most appropriate modeling framework for specific landscapes and climate regions.

4. Separating the numerical solver from the physicochemical calculations enables more controlled simulations where the specific impact of different processes can not only be properly quantified but also added or removed as needed for uncertainty analysis. Such model architecture is critical for model scalability by enabling the integration of new modules in a controlled manner.

The work presented here represents the first application of OpenWQ to improve water quality modeling, but there are many additional opportunities to build on this work. The case studies simulated here cover a range of pollution problems and hydrologic processes, but they are naturally limited in terms of the environments and contamination problems covered. The model simulations presented are also based on simple perturbation experiments, which were necessary for validation purposes; however, more comprehensive model applications should be carried out in the future for comparison with competing modeling approaches. The work presented also does not examine different numerical integration options. Research is needed to continue exploring the potential opportunities that OpenWQ creates for testing different biogeochemical, biophysical, and hydrologic processes and their model representations. Access to the OpenWQ source code and the case study tests is provided through the SUMMA website at `openwq.readthedocs.io`.

Acknowledgments

This work was supported by the NSERC-Alliance Grant ALLRP 571910-22. We acknowledge support from Environment and Climate Change Canada, the Global Water Futures programme, and the Natural Sciences and Engineering Research Council of Canada under Discovery Grant RGPN-2020-04467 (RJS).

Appendices

A Deriving analytical solutions for Tests 1 and 2: Single-species batch reaction

The single-species batch reactor tests contemplated involve (a) first-order decay and (b) second-order decay kinetics. Fig. 1 depicts the biogeochemical process. The analytical solution of a single species subject to first-order decay can be obtained by integrating Eq. 24 obtaining Eq. 25. In turn, the analytical solution of a single species subject to second-order decay can be obtained by integrating Eq. 26 obtaining Eq. 27.

$$\frac{dc_A}{dt} = -kc_A \tag{24}$$

$$\begin{gathered}
\frac{dc_A}{dt} = -kc_A \Leftrightarrow \frac{1}{c_A}dc_A = -kdt \Leftrightarrow \\
\int_0^t \frac{1}{c_A}dc_A = \int_0^t -kdt \Leftrightarrow \ln(c_A)\Big|_0^t = -kt\Big|_0^t \Leftrightarrow \\
\ln\left(c_A(t)\right) - \ln\left(c_A(0)\right) = -k\Delta t \Leftrightarrow \ln\left(\frac{c_A(t)}{c_A(0)}\right) = -k\Delta t \Leftrightarrow \\
\frac{c_A(t)}{c_A(0)} = -k\Delta t \Leftrightarrow c_A(t) = c_A(0)e^{-k\Delta t}
\end{gathered} \tag{25}$$

$$\frac{dc_A}{dt} = -kc_A^2 \tag{26}$$

$$\begin{gathered}
\frac{dc_A}{dt} = -kc_A^2 \Leftrightarrow \frac{1}{c_A^2}dc_A = -kdt \Leftrightarrow \\
\int_0^t c_A^{-2}dc_A = \int_0^t -kdt \Leftrightarrow -c_A^{-1}\Big|_0^t = -kt\Big|_0^t \Leftrightarrow \\
c_A^{-1}\Big|_0^t = kt\Big|_0^t \Leftrightarrow c_A(t)^{-1} - c_A(0)^{-1} = k\Delta t \Leftrightarrow \\
\frac{1}{c_A(t)} = \frac{1}{c_A(0)} + k\Delta t \Leftrightarrow c_A(t) = \frac{1}{\frac{1}{c_A(0)} + k\Delta t} \Leftrightarrow
\end{gathered} \tag{27}$$

B Deriving analytical solution for Test 3: Two-species reaction network

The two-species reaction network with linear decay is represented schematically in Fig. 2. Similarly to the single-species case above with first-order decay (Eq. 25), the fate of Species A in a two-species reaction network only depends on its own concentration and is given by Eq. 28.

$$c_A(t) = c_A(0)e^{(-k_A\Delta t)} \tag{28}$$

However, the fate of Species B depends on the time-evolution of concentrations of both Species A and B. This can be expressed as:

$$\frac{dc_B}{dt} = k_A c_A - k_B c_B \tag{29}$$

To derive the analytical solution of Eq. 29, we can start by replacing $c_A(t)$ by its analytical solution derived previously in Eq. 25. We obtain:

$$\begin{gathered}
\frac{dc_B}{dt} = k_A c_A(0)e^{(-k_A t)} - k_B c_B(t) \Leftrightarrow \\
\frac{dc_B}{dt} + k_B c_B = k_A c_A(0)e^{(-k_A t)}
\end{gathered} \tag{30}$$

The integrating factor, $e^{(k_B t)}$, can be used to integrate Eq. 30 by parts (i.e., $d(uv) = udv + vdu$). Multiplying Eq. 30 by the integrating factor, we obtain:

$$\begin{aligned} \frac{dc_B}{dt}e^{(k_B t)} + k_B c_B(t)e^{(k_B t)} = k_A c_A(0)e^{(-k_A t)}e^{(k_B t)} \Leftrightarrow \\ \frac{dc_B}{dt}e^{(k_B t)} + k_B c_B(t)e^{(k_B t)} = k_A c_A(0)e^{(k_B - k_A)t} \end{aligned} \tag{31}$$

Using the general expression for integration by parts and considering that functions u and v are given by $u = c_B$ and $v = e^{(k_B t)}$, we obtain:

$$d\Big(c_B e^{(k_B t)}\Big) = c_B d\Big(e^{(k_B t)}\Big) + e^{(k_B t)} dc_B \tag{32}$$

Replacing the derivative of $e^{(k_B t)}$ in Eq. 32, where $d\Big(e^{(k_B t)}\Big) = k_B e^{(k_B t)} dt$, leads to:

$$\begin{aligned} d(uv) = udv + vdu \Leftrightarrow \\ d\big(c_B e^{(k_B t)}\big) = c_B\big[k_B e^{(k_B t)} dt\big] + e^{(k_B t)} dc_B \end{aligned} \tag{33}$$

or

$$\frac{d}{dt}\big(c_B e^{(k_B t)}\big) = c_B k_B e^{(k_B t)} + e^{(k_B t)}\frac{dc_B}{dt} \tag{34}$$

The right-hand side of Eq. 34 is the same as the left-hand side of Eq. 31, so the same applies to the other side of the equations. Thus, we can re-write the equations as

$$\begin{aligned} \frac{d}{dt}\Big(c_B e^{(k_B t)}\Big) = k_A c_A(0)e^{(-k_A t)}e^{(k_B t)} \Leftrightarrow \\ \frac{d}{dt}\Big(c_B e^{(k_B t)}\Big) = k_A c_A(0)e^{\big[(k_B - k_A)t\big]} \Leftrightarrow \\ d\big(c_B e^{(k_B t)}\big) = k_A c_A(0)e^{\big[(k_B - k_A)t\big]} dt \end{aligned} \tag{35}$$

Integrating both sides of the equation, we obtain

$$\begin{aligned} \int_0^t d(c_B e^{(k_B t)}) = \int_0^t k_A c_A(0)e^{\big[(k_B - k_A)t\big]} dt \Leftrightarrow \\ c_B(t)e^{(k_B t)} = \frac{k_A c_A(0)}{k_B - k_A}e^{\big[(k_B - k_A)t\big]} + C', \end{aligned} \tag{36}$$

where C' is the integration constant. At $t = 0$, c_B becomes $c_B(0)$, so Eq. 36 can be written as

$$\begin{aligned} c_B(0)e^0 = \frac{k_A c_A(0)}{k_B - k_A}e^0 \Leftrightarrow \\ \Leftrightarrow C' = c_B(0) - \frac{k_A c_A(0)}{k_B - k_A}, \end{aligned} \tag{37}$$

which can be replaced in Eq. 36 to give:

$$\begin{aligned}
c_B(t)e^{(k_B t)} &= \frac{k_A c_A(0)}{k_B - k_A} e^{\left[(k_B - k_A)t\right]} + c_B(0) - \frac{k_A c_A(0)}{k_B - k_A} \Leftrightarrow \\
c_B(t)e^{(k_B t)} &= \frac{k_A c_A(0)}{k_B - k_A} \left[e^{\left[(k_B - k_A)t\right]} - 1 \right] + c_B(0) \Leftrightarrow \\
c_B(t) &= \frac{k_A c_A(0)}{k_B - k_A} \left[\frac{e^{\left[(k_B - k_A)t\right]}}{e^{(k_B t)}} - \frac{1}{e^{(k_B t)}} \right] + \frac{c_B(0)}{e^{(k_B t)}} \Leftrightarrow \\
c_B(t) &= \frac{k_A c_A(0)}{k_B - k_A} \left[e^{(-k_A t)} - e^{(-k_B t)} \right] + c_B(0)e^{(-k_B t)}
\end{aligned} \tag{38}$$

C Deriving analytical solution for Test 4: Three-species reaction network

A three-species reaction network with linear decay is represented schematically in Fig. 2. Concentrations of Species A and Species B are given by respectively Eqs. 28 and 36. The partial differential equation for the concentration of Species C can be written as:

$$\frac{dc_C}{dt} = k_B c_B - k_C c_C \tag{39}$$

The expression for $c_B(t)$ can be obtained from Eq. 36 and replaced in Eq. 40. We obtain:

$$\begin{aligned}
\frac{dc_C}{dt} &= k_B \left(\frac{k_A c_A(0)}{k_B - k_A} \left[e^{(-k_A t)} - e^{(-k_B t)} \right] + c_B(0)e^{(-k_B t)} \right) \\
&\qquad - k_C c_C \Leftrightarrow \\
\frac{dc_C}{dt} + k_C c_C &= k_B \left(\frac{k_A c_A(0)}{k_B - k_A} \left[e^{(-k_A t)} - e^{-k_B t} \right] + \right. \\
&\qquad \left. c_B(0)e^{(-k_B t)} \right)
\end{aligned} \tag{40}$$

The integrating factor used in Section B to enable integration of parts, $e^{(k_C t)}$, can be used here as well (i.e., $d(uv) = udv + vdu$). Multiplying Eq. 40 by this integrating factor, we obtain:

$$\begin{aligned}
&\frac{dc_C}{dt} e^{(k_C t)} + k_C c_C(t) e^{(k_C t)} = \\
&k_B \left(\frac{k_A c_A(0)}{k_B - k_A} \left[e^{(-k_A t)} - e^{(-k_B t)} \right] + c_B(0)e^{(-k_B t)} \right) e^{(k_C t)}
\end{aligned} \tag{41}$$

We can use the same expression derived to enable integration by parts in the previous case (Eq. 34) but replacing Species B by Species C: $\frac{d}{dt}\left(c_C e^{(k_C t)} \right) = c_C k_C e^{(k_C t)} + \frac{dc_C}{dt} e^{k_C t}$. Also, similarly to the previous case, the right-hand side of this equation is the same as the

left-hand side of Eq. 41, so the same applies to the other side of the equations. Thus, we can re-write the equations as follows:

$$\begin{aligned}
\frac{d}{dt}\Big(c_C e^{k_C t}\Big) &= k_B\Bigg(\frac{k_A c_A(0)}{k_B - k_A}\Big[e^{-k_A t} - e^{-k_B t}\Big] + \\
&\qquad c_B(0)e^{-k_B t}\Bigg)e^{(k_C t)} \Leftrightarrow \\
d\Big(c_C e^{k_C t}\Big) &= k_B\Bigg(\frac{k_A c_A(0)}{k_B - k_A}\Big[e^{-k_A t} - e^{-k_B t}\Big] + \\
&\qquad c_B(0)e^{-k_B t}\Bigg)e^{(k_C t)}dt \Leftrightarrow \\
d\Big(c_C e^{k_C t}\Big) &= k_B\Bigg(\frac{k_A c_A(0)}{k_B - k_A}\Big[e^{(k_C - k_A)t} - e^{(k_C - k_B)t}\Big] + \\
&\qquad c_B(0)e^{(k_C - k_B)t}\Bigg)dt
\end{aligned} \tag{42}$$

Integrating both sides of the equation we obtain:

$$\begin{aligned}
\int_0^t d\big(c_C e^{(k_C t)}\big) &= \\
\int_0^t \Bigg[k_B\Bigg(\frac{k_A c_A(0)}{k_B - k_A}\Big[e^{\left[(k_C - k_A)t\right]} - e^{\left[(k_C - k_B)t\right]}\Big] + \\
&\qquad c_B(0)e^{\left[(k_C - k_B)t\right]}\Bigg)\Bigg] \Leftrightarrow \\
c_C(t)e^{(k_C t)} &= k_B\Bigg(\frac{k_A c_A(0)}{k_B - k_A}\Big[\frac{1}{k_C - k_A}e^{\left[(k_C - k_A)t\right]} - \\
\frac{1}{k_C - k_B}e^{\left[(k_C - k_B)t\right]}\Big] &+ \frac{c_B(0)}{k_C - k_B}e^{\left[(k_C - k_B)t\right]}\Bigg) + C'',
\end{aligned} \tag{43}$$

where C" is the integration constant. At $t = 0$, c_C becomes $c_C(t)$, so Eq. 43 becomes

$$
\begin{aligned}
c_C(0)e^{(k_C 0)} = k_B\Bigg(\frac{k_A c_A(0)}{k_B - k_A}\Big[\frac{1}{k_C - k_A}e^0 - \\
\frac{1}{k_C - k_B}e^{\left[(k_C - k_B)0\right]}\Big] + \frac{c_B(0)}{k_C - k_B}e^0\Bigg) + C'' \Leftrightarrow \\
c_C(0)1 = k_B\Bigg(\frac{k_A c_A(0)}{k_B - k_A}\Big[\frac{1}{k_C - k_A}1 - \\
\frac{1}{k_C - k_B}1\Big] + \frac{c_B(0)}{k_C - k_B}1\Bigg) + C'' \Leftrightarrow C'' = \\
c_C(0) - k_B\Bigg(\frac{k_A c_A(0)}{k_B - k_A}\Big[\frac{1}{k_C - k_A} - \frac{1}{k_C - k_B}\Big] + \\
\frac{c_B(0)}{k_C - k_B}\Bigg),
\end{aligned}
\tag{44}
$$

which can be replaced in Eq. 43 to give:

$$
\begin{aligned}
c_C(t)e^{(k_C t)} = k_B\Bigg(\frac{k_A c_A(0)}{k_B - k_A}\Big[\frac{1}{k_C - k_A}e^{\left[(k_C - k_A)t\right]} - \\
\frac{1}{k_C - k_B}e^{\left[(k_C - k_B)t\right]}\Big] + \frac{c_B(0)}{k_C - k_B}e^{\left[(k_C - k_B)t\right]}\Bigg) + \\
c_C(0) - k_B\Bigg(\frac{k_A c_A(0)}{k_B - k_A}\Big[\frac{1}{k_C - k_A} - \frac{1}{k_C - k_B}\Big] + \frac{c_B(0)}{k_C - k_B}\Bigg)
\end{aligned}
\tag{45}
$$

This can be rearranged to give:

$$
\begin{aligned}
c_C(t) = k_B\Bigg(\frac{k_A c_A(0)}{k_B - k_A}\Big[\frac{1}{k_C - k_A}e^{(-k_A t)} - \frac{1}{k_C - k_B}e^{(-k_B t)}\Big] + \\
\frac{c_B(0)}{k_C - k_B}e^{(-k_B t)}\Bigg) + \\
c_C(0)e^{(-k_C t)} - k_B\Bigg(\frac{k_A c_A(0)}{k_B - k_A}\Big[\frac{1}{k_C - k_A} - \frac{1}{k_C - k_B}\Big] + \\
\frac{c_B(0)}{k_C - k_B}\Bigg)e^{(-k_C t)},
\end{aligned}
\tag{46}
$$

and then simplified to:

$$
\begin{aligned}
c_C(t) = k_B\Bigg(\frac{k_A c_A(0)}{k_B - k_A}\Big[\frac{e^{(-k_A t)}}{k_C - k_A} - \\
\frac{e^{(-k_B t)}}{k_C - k_B}\Big] + \frac{c_B(0)e^{(-k_B t)}}{k_C - k_B}\Bigg) + c_C(0)e^{(-k_C t)} - \\
k_B\Bigg(\frac{k_A c_A(0)}{k_B - k_A}\Big[\frac{e^{(-k_C t)}}{k_C - k_A} - \frac{e^{(-k_C t)}}{k_C - k_B}\Big] + \frac{c_B(0)e^{(-k_C t)}}{k_C - k_B}\Bigg)
\end{aligned}
\tag{47}
$$

D Deriving analytical solution for Test 5: Nitrogen cycle

The simulation of the nitrogen cycle is very common in freshwater water quality studies because it allows for addressing issues with nutrient pollution and eutrophication. The nitrogen cycle simulated involves different nitrogen species (Fig. 4). The conceptual cycling framework used is similar to that used in catchment-scale models like HYPE Lindström et al. (2010), CRHM-WQ (Costa et al., 2021) models, SWAT (Arnold et al., 2012), and INCA ("A semi-distributed ntegrated itrogen model for multiple source assessment in tchments (INCA): Part I — model structure and process equations", 1998). The analytical solutions for the different nitrogen species can be obtained directly (or derived) from Eq. 28, Eq. 38, or Eq. 47 depending on their positioning in the reaction chain:

1. **refractoryN** ($Nref$): Similar to Eq. 28, which for this specific process and N species reads as:

$$c_{Nref}(t) = c_{Nref}(0)e^{\left[-(k_{degr}+k_{diss1})t\right]} \tag{48}$$

2. **labileN** ($Nref$): Similar to Eq. 36, which for this specific processes and N species reads as:

$$c_{Nlab}(t) = \frac{k_{degr}c_{Nref}(0)}{k_{min}+k_{diss2}-k_{degr}}\left[e^{(-k_{degr}t)} - e^{\left[-(k_{min}+k_{diss2})t\right]}\right] + c_{Nlab}(0)e^{\left[-(k_{min}+k_{diss2})t\right]} \tag{49}$$

3. **DON**: Needs specific derivation using Eqs. 28 and 36 (see below)
4. **DIN**: Needs specific derivation using Eqs. 49 and 28 (see below)

DON The concentration of DON does not depend on itself, but rather on the evolution of the concentration of $Nref$ and $Nlab$. The differential equation can be written as:

$$\frac{dc_{DON}}{dt} = k_{diss1}c_{Nref} + k_{diss2}c_{Nlab} \tag{50}$$

Analytical solutions suitable for c_{Nref} and c_{Nlab}, due to their positioning in the rection chain, have been derived before (Eqs. 28 and 38, respectively). These solutions can be replaced in Eq. 50.

$$\begin{aligned}\frac{dc_{DON}}{dt} &= k_{diss1}\left[c_{Nref}e^{\left[-(k_{degr}+k_{diss1})t\right]}\right] \\ &+k_{diss2}\left[\frac{k_{degr}c_{Nref}}{k_{min}+k_{diss2}-k_{degr}}\left(e^{(-k_{degr}t)} - \right.\right. \\ &\left.\left.e^{\left[-(k_{min}+k_{diss2})t\right]}\right) + c_{Nlab}(0)e^{\left[-(k_{min}+k_{diss2})t\right]}\right]\end{aligned} \tag{51}$$

Since this solution is independent of the concentration of DON, it can be integrated in its current state.

$$
\begin{aligned}
dc_{DON} = k_{diss1}\left[c_{Nref}e^{\left[-(k_{degr}+k_{diss1})t\right]}\right]dt \\
+k_{diss2}\left[\frac{k_{degr}c_{Nref}}{k_{min}+k_{diss2}-k_{degrd}}\left(e^{(-k_{degr}t)}- \right.\right. \\
\left.\left.e^{\left[-(k_{min}+k_{diss2})t\right]}\right)+c_{Nlab}(0)e^{\left[-(k_{min}+k_{diss2})t\right]}\right]dt \Leftrightarrow \\
c_{DON}(t) = \frac{k_{diss1}c_{Nref}(t)}{-(k_{degr}+k_{diss1})}e^{\left[-(k_{degr}+k_{diss1})t\right]}+ \\
\frac{k_{diss2}k_{degr}c_{Nref}(t)}{k_{min}+k_{diss2}-k_{degr}}\left(\frac{e^{(-k_{degr}t)}}{-k_{degr}}-\frac{e^{\left[-(k_{min}+k_{diss2})t\right]}}{-(k_{min}+k_{diss2})}\right)+ \\
\frac{k_{diss2}c_{Nlab}(0)}{-(k_{min}+k_{diss2})}e^{\left[-(k_{min}+k_{diss2})t\right]}+C'''
\end{aligned}
\tag{52}
$$

Considering that at $t = 0$, $c_{DON}(t)$ becomes $c_{DON}(0)$, we can determine C''' as follows:

$$
\begin{aligned}
C''' = c_{DON}(0)+\frac{k_{diss1}c_{Nref}(t)}{k_{degr}+k_{diss1}}- \\
\frac{k_{diss2}k_{degr}c_{Nref}(t)}{k_{min}+k_{diss2}-k_{degr}}\left(\frac{1}{-k_{degr}}-\frac{1}{-(k_{min}+k_{diss2})}\right)+ \\
\frac{k_{diss2}c_{Nlab}(0)}{-(k_{min}+k_{diss2})}
\end{aligned}
\tag{53}
$$

Replacing Eq. 53 into Eq. 52 we obtain:

$$
\begin{aligned}
c_{DON}(t) = \frac{k_{diss1}c_{Nref}(t)}{-(k_{degr}+k_{diss1})}e^{\left[-(k_{degr}+k_{diss1})t\right]} \\
+\frac{k_{diss2}k_{degr}c_{Nref}(t)}{k_{min}+k_{diss2}-k_{degr}}\left(\frac{e^{(-k_{degr}t)}}{-k_{degr}}- \right. \\
\left.\frac{e^{\left[-(k_{min}+k_{diss2})t\right]}}{-(k_{min}+k_{diss2})}\right)+\frac{k_{diss2}c_{Nlab}(0)}{-(k_{min}+k_{diss2})} \\
e^{\left[-(k_{min}+k_{diss2})t\right]}+c_{DON}(0)+\frac{k_{diss1}c_{Nref}(t)}{k_{degr}+k_{diss1}} \\
-\frac{k_{diss2}k_{degr}c_{Nref}(t)}{k_{min}+k_{diss2}-k_{degr}}\left(\frac{1}{-k_{degr}}- \right. \\
\left.\frac{1}{-(k_{min}+k_{diss2})}\right)+\frac{k_{diss2}c_{Nlab}(0)}{-(k_{min}+k_{diss2})}
\end{aligned}
\tag{54}
$$

Eq. 54 can be simplified to obtain:

$$
\begin{aligned}
c_{DON}(t) = -\frac{k_{diss1}c_{Nref}(t)}{k_{degr}+k_{diss1}}e^{\left[-(k_{degr}+k_{diss1})t\right]}+ \\
\frac{k_{diss2}k_{degr}c_{Nref}(t)}{k_{min}+k_{diss2}-k_{degr}}\left(\frac{e^{\left[k_{min}+k_{diss2}t\right]}}{k_{min}+k_{diss2}}- \\
\frac{e^{(-k_{degr}t)}}{k_{degr}}\right)-\frac{k_{diss2}c_{Nlab}(0)}{k_{min}+k_{diss2}} \\
e^{\left[-(k_{min}+k_{diss2})t\right]}+c_{DON}(0)+ \\
\frac{k_{diss1}c_{Nref}(t)}{k_{degr}+k_{diss1}}-\frac{k_{diss2}k_{degr}c_{Nref}(t)}{k_{min}+k_{diss2}-k_{degr}} \\
\left(\frac{1}{k_{min}+k_{diss2}}-\frac{1}{k_{degr}}\right)-\frac{k_{diss2}c_{Nlab}(0)}{k_{min}+k_{diss2}}
\end{aligned}
\tag{55}
$$

DIN The ordinary differential equation for DIN can be written as:

$$
\frac{dc_{DIN}}{dt} = k_{min}c_{Nlab} - (k_{denit}+k_{plantup})c_{DIN} \tag{56}
$$

The concentration of $c_{Nlab}(t)$ has been derived above in Eq. 49 and can be replaced in Eq. 56 to give:

$$
\begin{aligned}
\frac{dc_{DIN}}{dt} = k_{min}\left(\frac{k_{degr}c_{(Nref,0)}}{k_{min}+k_{diss2}-k_{degr}}\left[e^{(-k_{degr}t)}- \right.\right. \\
\left.\left.e^{\left[-(k_{min}+k_{diss2})t\right]}\right]+c_{Nlab}(0)e^{\left[-(k_{min}+k_{diss2})t\right]}\right)- \\
(k_{denit}+k_{plantup})c_{DIN}(t) \Leftrightarrow \\
\frac{dc_{DIN}}{dt} = \frac{k_{min}k_{degr}c_{(Nref,0)}}{k_{min}+k_{diss2}-k_{degr}}\left[e^{(-k_{degr}t)}- \right. \\
\left.e^{\left[-(k_{min}+k_{diss2})t\right]}\right]+k_{min}c_{Nlab}(0) \\
e^{\left[-(k_{min}+k_{diss2})t\right]}-(k_{denit}+k_{plantup})c_{DIN}
\end{aligned}
\tag{57}
$$

The same integrating factor used before, which in this context reads $e^{\left[(k_{denit}+k_{plantup})t\right]}$, can be used here to allow similar integration by parts (i.e., $d(uv) = udv + vdu$). Multiplying Eq. 57 by the integration factor, we obtain:

$$
\begin{aligned}
\frac{dc_{DIN}}{dt}e^{\left[(k_{denit}+k_{plantup})t\right]}+(k_{denit}+k_{plantup}) \\
c_{DIN}(t)e^{\left[(k_{denit}+k_{plantup})t\right]} \\
= \frac{k_{min}k_{degr}c_{Nref}(0)}{k_{min}+k_{diss2}-k_{degr}}\left[e^{(-k_{degr}t)}-e^{\left[-(k_{min}+k_{diss2})t\right]}\right] \\
e^{\left[(k_{denit}+k_{plantup})t\right]}+k_{min}c_{Nlab}(0)e^{\left[-(k_{min}+k_{diss2})t\right]} \\
e^{\left[(k_{denit}+k_{plantup})t\right]}
\end{aligned}
\tag{58}
$$

Now we can use the same expression derived for integration by parts of previous cases (i.e., Eq. 34) and adapt it to DIN and the respective transformations:

$$\frac{d}{dt}\Big[c_{DIN}e^{\big((k_{denit}+k_{plantup})t\big)}\Big] = \frac{dc_{DIN}}{dt}e^{\Big[(k_{denit}+k_{plantup})t\Big]} + (k_{denit}+k_{plantup})c_{DIN}e^{\Big[(k_{denit}+k_{plantup})t\Big]} \tag{59}$$

Similarly to previous cases, the right-hand side of this equation is the same as the left-hand side of Eq. 57, so the same applies to the other side of the equations so that we can re-write the equations as:

$$\begin{aligned}\frac{d}{dt}\left(c_{DIN}e^{\Big[(k_{denit}+k_{plantup})t\Big]}\right) &= \frac{k_{min}k_{degr}c_{Nref}(0)}{k_{min}+k_{diss2}-k_{degr}} \\ &\left[e^{(-k_{degr}t)} - e^{\Big[-(k_{min}+k_{diss2})t\Big]}\right]e^{\Big[(k_{denit}+k_{plantup})t\Big]} + \\ &k_{min}c_{Nlab}(0)e^{\Big[-(k_{min}+k_{diss2})t\Big]}e^{\Big[(k_{denit}+k_{plantup})t\Big]} \Leftrightarrow \\ d\big(c_{DIN}e^{\Big[(k_{denit}+k_{plantup})t\Big]}\big) &= \left(\frac{k_{min}k_{degr}c_{Nref}(0)}{k_{min}+k_{diss2}-k_{degr}}\right. \\ &\left[e^{\Big[((k_{denit}+k_{plantup})-k_{degr})t\Big]} - e^{\Big[(k_{denit}+k_{plantup}-k_{min}-k_{diss2})t\Big]}\right] \\ &\left.+k_{min}c_{Nlab}(0)e^{\Big[(k_{denit}+k_{plantup}-k_{min}-k_{diss2})t\Big]}\right)dt\end{aligned} \tag{60}$$

Now we can integrate the equation with respect to $c_{DIN}(t)$ and t:

$$\begin{aligned}\int d\left(c_{DIN}e^{\Big[(k_{denit}+k_{plantup})t\Big]}\right) &= \int\left(\frac{k_{min}k_{degr}c_{Nref}(0)}{k_{min}+k_{diss2}-k_{degr}}\right. \\ &\left[e^{\Big[(k_{denit}+k_{plantup}-k_{degr})t\Big]} - e^{\Big[(k_{denit}+k_{plantup}-k_{min}-k_{diss2})t\Big]}\right] \\ &\left.+k_{min}c_{Nlab}(0)e^{\Big[(k_{denit}+k_{plantup}-k_{min}-k_{diss2})t\Big]}\right)dt \Leftrightarrow \\ c_{DIN}(t)e^{\Big[(k_{denit}+k_{plantup})t\Big]} &= \frac{k_{min}k_{degr}c_{Nref}(0)}{k_{min}+k_{diss2}-k_{degr}} \\ &\left[\frac{e^{\Big[(k_{denit}+k_{plantup}-k_{degr})t\Big]}}{k_{denit}+k_{plantup}-k_{degr}} - \frac{e^{\Big[(k_{denit}+k_{plantup}-k_{min}-k_{diss2})t\Big]}}{(k_{denit}+k_{plantup})-k_{min}-k_{diss2}}\right] \\ &+k_{min}c_{Nlab}(0)\frac{e^{\Big[(k_{denit}+k_{plantup}-k_{min}-k_{diss2})t\Big]}}{(k_{denit}+k_{plantup}-k_{min}-k_{diss}} + C''''\end{aligned} \tag{61}$$

Considering that at $t = 0$, $c_{DIN}(t)$ becomes $c_{DIN}(0)$, we can determine the constant C'''' as follows:

$$C'''' = c_{DIN}(0) - \frac{k_{miner}k_{degr}c_{Nref}(0)}{k_{min} + k_{diss2} - k_{degr}} \left[\frac{1}{(k_{denit} + k_{plantup}) - k_{degr}} - \frac{1}{(k_{denit} + k_{plantup}) - k_{min} - k_{diss2}} \right] - k_{miner}c_{Nlab}(0) \frac{1}{(k_{denit} + k_{plantup}) - k_{min} - k_{diss2}} \tag{62}$$

Replacing the integrating constant in Eq. 61 we obtain:

$$\begin{aligned} c_{DIN}(t)e^{\left[(k_{denit}+k_{plantup})t\right]} &= \frac{k_{min}k_{degr}c_{Nref}(0)}{k_{min} + k_{diss2} - k_{degr}} \left[\frac{e^{\left[(k_{denit}+k_{plantup}-k_{degr})t\right]}}{k_{denitr} + k_{plantup} - k_{degr}} - \frac{e^{\left[(k_{denit}+k_{plantup}-k_{min}-k_{diss2})t\right]}}{k_{denit} + k_{plantup} - k_{min} - k_{diss2}} \right] \\ &+ k_{min}c_{Nlab}(0) \frac{e^{\left[(k_{denit}+k_{plantup}-k_{min}-k_{diss2})t\right]}}{k_{denit} + k_{plantup} - k_{min} - k_{diss2}} \\ &+ c_{DIN}(0) - \frac{k_{min}k_{degr}c_{Nref}(0)}{k_{min} + k_{diss2} - k_{degr}} \left[\frac{1}{k_{denit} + k_{plantup} - k_{degr}} \right. \\ &\left. - \frac{1}{k_{denit} + k_{plantup} - k_{min} - k_{diss2}} \right] - k_{min}c_{Nlab}(0) \\ &\left(\frac{1}{k_{denit} + k_{plantup} - k_{min} - k_{diss2}} \right) \end{aligned} \tag{63}$$

E Deriving analytical solution for Test 6: DO-BOD cycle

Dissolved oxygen (DO) depletion in rivers and lakes is a common consequence of pollution. It typically occurs near discharge outlets of untreated wastewater, which can lead to high levels of organic matter that, during decomposition by aerobic bacteria, causes a DO sag in the water column. For purposes of DO dynamics, such organic matter is typically translated into units of biological oxygen demand (BOD). Fig. 5 depicts the processes involved, and the Streeter–Phelps equation (Streeter & Phelps, 1925) has long been derived for such problems. It reads:

$$\frac{dD}{dt} = k_1 L_t - k_2 D \tag{64}$$

The equation states that the total change in oxygen deficit (D) is equal to the difference between the two rates of deoxygenation and reaeration at any time. The derivation of the Streeter–Phelps equation is well known, so it won't be repeated here.

$$D = \frac{k_1 L_a}{k_2 - k_1}(e^{(-k_1 t)} - e^{(-k_2 t)}) + D_a e^{(-k_2 t)} \tag{65}$$

where D is the saturation deficit in g/m^3, which can be derived from the dissolved oxygen concentration at saturation minus the actual dissolved oxygen concentration ($D = DO_{sat} - DO$); k_1 is the deoxygenation rate, usually in d^{-1}; k_2 is the reaeration rate, usually in d^{-1}; L_a is the initial oxygen demand of organic matter in the water, also called the ultimate BOD (BOD at time $t = \infty$). The unit of L_a is g/m^3; k_1; L_t is the oxygen demand remaining at time t, $L_t = L_a e^{(-k_1 t)}$; D_a is the initial oxygen deficit $[g/m^3]$; and t is the elapsed time in days.

F Reactive and non-reactive transport: Instantaneous point source (Tests 7 and 8)

The general 1D advection-dispersion-reaction partial differential equation is given by

$$\frac{\partial c}{\partial t} = D_x \frac{\partial^2 c}{\partial x^2} - \nu \frac{\partial c}{\partial x} - \lambda c \tag{66}$$

where c is the concentration of the tracer, t is time, D_x is the dispersion coefficient in the flow direction, x is the distance in the flow direction, ν is the flow velocity in the x direction, and λ is a linear reaction term that can be set to zero for non-reactive tracers. Various analytical solutions for Eq. 66 have been derived and compiled by Wexler (1992) for different idealized scenarios.

Eq. 66 has been modified by Wexler (1992) to include an instantaneous point source and it reads:

$$\frac{\partial c}{\partial t} = D_x \frac{\partial^2 c}{\partial x^2} - \nu \frac{\partial c}{\partial x} - \lambda c + \frac{Q}{n} \partial t c_0 \delta(x - x_c) \delta(t - t'_c) \tag{67}$$

where t'_c is the time at which the instantaneous point source is activated, Q is the fluid injection rate, n is the aquifer porosity, δ is the Dirac delta (impulse) function, and x_c is the location of the instantaneous point source. The analytical solution to Eq. 67 has been derived by Bear (1979) considering the following boundary conditions and initial conditions.

1. Boundary conditions (Neumann or second-type):
   $c, \nabla c = 0, \quad x = \pm\infty; y = \pm\infty$
2. Initial conditions:
   $c^{t=0} = 0, \quad -\infty < x < \infty; -\infty < y < \infty,$

Eq. 68 shows the resulting analytical solution that can be used for solutes that are non-reactive (Test 7) or reactive (Test 8) by simply setting $\lambda = 0$ in the former (Test 7).

$$\begin{aligned} c(x) = & \frac{c_0 Q}{4n\pi\gamma D_x} \exp\left[\frac{\nu(x - x_0)}{2D_x}\right] \\ & \frac{1}{t} \exp\left[-\left(\frac{\nu^2}{4D_x}\right)\tau - \frac{(x - Xc)^2}{4D_x \tau}\right], \end{aligned} \tag{68}$$

The equation assumes that (1) the fluid has constant density and viscosity, (2) the solute may be subject to first-order chemical transformation, (3) the flow is uniform in the x-direction only, (4) the flow velocity is constant, and (5) the longitudinal dispersion coefficient (D) is constant. The solution has a mathematical singularity in the point source region (Abdelaziz et al., 2013) because it takes the form of the exponential integral when both $x - x_c$ approaches zero, hence becoming infinite at $\tau = 0$. However, according to Wexler (1989) the solution is still valid as long as $(x - x_c)^2$ is larger than ν^2, as it is the case in our simulation tests.

G Reactive and non-reactive transport: Continuous point source (Tests 9 and 10)

The analytical solution for the transport of solutes with a continuous point source has been derived in Wexler (1992) after modification from Bear (1979) and Genuchten & Alves (1982).

$$c(x) = \frac{c_0}{2}\Bigg\{ \exp\left[\frac{x}{2D_x}(\nu - U)\right]\operatorname{erfc}\left[\frac{x - Ut}{2\sqrt{D_x t}}\right] + \exp\left[\frac{x}{2D_x}(\nu + U)\right]\operatorname{erfc}\left[\frac{x + Ut}{2\sqrt{D_x t}}\right]\Bigg\} \tag{69}$$

where c_0 is the concentration of the continuous point source, $U = \sqrt{\nu^2 + 4\lambda D}$ and erfc is the complementary error function. Parameter λ is the first-order reaction rate used for Test 10, which can be set to zero for Test 9.

References

Abdelaziz, R., Pearson, A., & Merkel, B. (2013). Lattice Boltzmann modeling for tracer test analysis in a fractured Gneiss aquifer. *Natural Science*, *5*, 368-374. doi: 10.4236/ns.2013.53050

Alexander, A. C., Levenstein, B., Sanderson, L. A., Blukacz-Richards, E. A., & Chambers, P. A. (2020). How does climate variability affect water quality dynamics in canada's oil sands region? *Science of The Total Environment*, *732*, 139062. doi: https://doi.org/10.1016/j.scitotenv.2020.139062

Arnold, J. G., Moriasi, D. N., Gassman, P. W., Abbaspour, K. C., White, M. J., Srinivasan, R., ... Jha, M. K. (2012). SWAT: Model Use, Calibration, and Validation. *Trans. ASABE*, *55*(4), 1491–1508.

Bear, J. (1979). *Hydraulics of groundwater*. McGraw-Hill series in water resources and environmental engineering. McGraw-Hill, New York.

Beven, K. (2006). A manifesto for the equifinality thesis. *Journal of Hydrology*, *320*(1), 18-36. (The model parameter estimation experiment) doi: https://doi.org/10.1016/j.jhydrol.2005.07.007

Bussi, G., Janes, V., Whitehead, P. G., Dadson, S. J., & Holman, I. P. (2017). Dynamic response of land use and river nutrient concentration to long-term climatic changes. *The Science of the total environment*, *590-591*, 818-831. doi: 10.1016/j.scitotenv.2017.03.069

Bussi, G., Whitehead, P. G., Jin, L., Taye, M. T., Dyer, E., Hirpa, F. A., ... Charles, K. J. (2021). Impacts of climate change and population growth on river nutrient loads in a data scarce region: The upper awash river (ethiopia). *Sustainability*, *13*. doi: 10.3390/su13031254

Celia, M. A., Bouloutas, E. T., & Zarba, R. L. (1990). A general mass-conservative numerical solution for the unsaturated flow equation. *Water Resources Research*, *26*(7), 1483-1496. doi: https://doi.org/10.1029/WR026i007p01483

Charlton, M. B., Bowes, M. J., Hutchins, M. G., Orr, H. G., Soley, R., & Davison, P. (2018). Mapping eutrophication risk from climate change: Future phosphorus concentrations in english rivers. *Science of The Total Environment*, *613-614*, 1510-1526. doi: https://doi.org/10.1016/j.scitotenv.2017.07.218

Clark, M. P., Nijssen, B., Lundquist, J. D., Kavetski, D., Rupp, D. E., Woods, R. A., ... Rasmussen, R. M. (2015a). A unified approach for process-based hydrologic modeling: 1. modeling concept. *Water Resources Research*, *51*(4), 2498-2514. Retrieved from `https://agupubs.onlinelibrary.wiley.com/doi/abs/10.1002/2015WR017198` doi: https://doi.org/10.1002/2015WR017198

Clark, M. P., Nijssen, B., Lundquist, J. D., Kavetski, D., Rupp, D. E., Woods, R. A., ... Marks, D. G. (2015b). A unified approach for process-based hydrologic modeling: 2. model implementation and case studies. *Water Resources Research*, *51*(4), 2515-2542. Retrieved from `https://agupubs.onlinelibrary.wiley.com/doi/abs/10.1002/2015WR017200` doi: https://doi.org/10.1002/2015WR017200

Clark, M. P., Zolfaghari, R., Green, K. R., Trim, S., Knoben, W. J. M., Bennett, A., ... Spiteri, R. J. (2021a). The numerical implementation of land models: Problem

formulation and laugh tests. *Journal of Hydrometeorology*, *22*(6), 1627 - 1648. doi: 10.1175/JHM-D-20-0175.1

Clark, M. P., Zolfaghari, R., Green, K. R., Trim, S., Knoben, W. J. M., Bennett, A., ... Spiteri, R. J. (2021b). The numerical implementation of land models: Problem formulation and laugh tests. *Journal of Hydrometeorology*, *22*(6), 1627 - 1648. doi: https://doi.org/10.1175/JHM-D-20-0175.1

Costa, D., Baulch, H., Elliott, J., Pomeroy, J., & Wheater, H. (2020). Modelling nutrient dynamics in cold agricultural catchments: A review. *Environmental Modelling & Software*, *124*, 104586. doi: https://doi.org/10.1016/j.envsoft.2019.104586

Costa, D., Pomeroy, J. W., Brown, T., Baulch, H., Elliott, J., & Macrae, M. (2021). Advances in the simulation of nutrient dynamics in cold climate agricultural basins: Developing new nitrogen and phosphorus modules for the Cold Regions Hydrological Modelling Platform. *Journal of Hydrology*, *603*, 126901. doi: https://doi.org/10.1016/j.jhydrol.2021.126901

Costa, D., Sutter, C., Shepherd, A., Jarvie, H., Wilson, H., Elliott, J., ... Macrae, M. (2022). Impact of climate change on catchment nutrient dynamics: insights from around the world. *Environmental Reviews*, *0*(0), null. doi: 10.1139/er-2021-0109

Crossman, J., Futter, M. N., Whitehead, P. G., Stainsby, E., Baulch, H. M., Jin, L., ... Dillon, P. J. (2014). Flow pathways and nutrient transport mechanisms drive hydrochemical sensitivity to climate change across catchments with different geology and topography. *Hydrol. Earth Syst. Sci.*, *18*, 5125-5148. doi: 10.5194/hess-18-5125-2014

Effects of lake water level fluctuation due to drought and extreme winter precipitation on mixing and water quality of an alpine lake, case study: Lake arrowhead, california. (2020). *Science of The Total Environment*, *714*, 136762. doi: https://doi.org/10.1016/j.scitotenv.2020.136762

El-Khoury, A., Seidou, O., Lapen, D. R., Que, Z., Mohammadian, M., Sunohara, M., & Bahram, D. (2015). Combined impacts of future climate and land use changes on discharge, nitrogen and phosphorus loads for a canadian river basin. *Journal of Environmental Management*, *151*, 76-86. doi: https://doi.org/10.1016/j.jenvman.2014.12.012

Ervinia, A., Huang, J., & Zhang, Z. (2020). Nitrogen sources, processes, and associated impacts of climate and land-use changes in a coastal china watershed: Insights from the inca-n model. *Marine Pollution Bulletin*, *159*, 111502. doi: https://doi.org/10.1016/j.marpolbul.2020.111502

Field, C. B., & Barros, V. R. (2014). *Climate change 2014: Impacts, adaptation, and vulnerability: Working group ii contribution to the fifth assessment report of the intergovernmental panel on climate change* (Tech. Rep.).

Genuchten, M. T., & Alves, W. (1982). *Analytical solutions of the one-dimensional convective-dispersive solute transport equation.* US Department of Agriculture.

Jarsjö, J., Törnqvist, R., & Su, Y. (2017). Climate-driven change of nitrogen retention–attenuation near irrigated fields: multi-model projections for central asia. *Environmental Earth Sciences*, *76*, 117. doi: 10.1007/s12665-017-6418-y

Jeppesen, E., Kronvang, B., Olesen, J. E., Audet, J., Søndergaard, M., Hoffmann, C. C., ... Özkan, K. (2011). Climate change effects on nitrogen loading from cultivated catchments in europe: implications for nitrogen retention, ecological state of lakes and adaptation. *Hydrobiologia*, *663*, 1-21. doi: 10.1007/s10750-010-0547-6

Lindström, G., Pers, C., Rosberg, J., Strömqvist, J., & Arheimer, B. (2010). Development and testing of the HYPE (Hydrological Predictions for the Environment) water quality model for different spatial scales. *Hydrology Research*, *41*(3-4), 295. doi: 10.2166/nh.2010.007

Luo, C., Li, Z., Liu, H., Li, H., Wan, R., Pan, J., & Chen, X. (2020). Differences in the responses of flow and nutrient load to isolated and coupled future climate and land use changes. *Journal of Environmental Management*, *256*, 109918. doi: https://doi.org/10.1016/j.jenvman.2019.109918

Ockenden, M. C., Deasy, C. E., Benskin, C., Beven, K. J., Burke, S., Collins, A. L., ... Haygarth, P. M. (2016). Changing climate and nutrient transfers: Evidence from high temporal resolution concentration-flow dynamics in headwater catchments. *Science of The Total Environment*, *548-549*, 325-339. doi: https://doi.org/10.1016/j.scitotenv.2015.12.086

Ockenden, M. C., Hollaway, M. J., Beven, K. J., Collins, A. L., Evans, R., Falloon, P. D., ... Haygarth, P. M. (2017). Major agricultural changes required to mitigate phosphorus losses under climate change. *Nature Communications*, *8*, 161. doi: 10.1038/s41467-017-00232-0

Onishi, T., Yoshino, J., Hiramatsu, K., & Somura, H. (2020). Developing a hydro-chemical model of ise bay watersheds and the evaluation of climate change impacts on discharge and nitrate-nitrogen loads. *Limnology*, *21*, 465-486. doi: 10.1007/s10201-020-00622-2

Partow, A. (1999). *ExprTk C++ Mathematical Expression Library.*

Pomeroy, J., Brown, T., Fang, X., Shook, K., Pradhananga, D., Armstrong, R., ... Lopez Moreno, J. (2022). The cold regions hydrological modelling platform for hydrological diagnosis and prediction based on process understanding. *Journal of Hydrology*, *615*, 128711. doi: https://doi.org/10.1016/j.jhydrol.2022.128711

Pomeroy, J. W., Gray, D. M., Brown, T., Hedstrom, N. R., Quinton, W. L., Granger, R. J., & Carey, S. K. (2007). The cold regions hydrological model: A platform for basing process representation and model structure on physical evidence. *Hydrological Processes*, *21*(19), 2650–2667. doi: {10.1002/hyp.6787}

Raimonet, M., Thieu, V., Silvestre, M., Oudin, L., Rabouille, C., Vautard, R., & Garnier, J. (2018). Landward perspective of coastal eutrophication potential under future climate change: The seine river case (france). *Frontiers in Marine Science*, *5*, 136.

Reggiani, P., Sivapalan, M., & Majid Hassanizadeh, S. (1998). A unifying framework for watershed thermodynamics: balance equations for mass, momentum, energy and entropy, and the second law of thermodynamics. *Advances in Water Resources*, *22*(4), 367-398. doi: https://doi.org/10.1016/S0309-1708(98)00012-8

Renard, B., Kavetski, D., Kuczera, G., Thyer, M., & Franks, S. W. (2010). Understanding predictive uncertainty in hydrologic modeling: The challenge of identifying input and structural errors. *Water Resources Research*, *46*(5). doi: https://doi.org/10.1029/2009WR008328

Rood, S. B., Pan, J., Gill, K. M., Franks, C. G., Samuelson, G. M., & Shepherd, A. (2008). Declining summer flows of rocky mountain rivers: Changing seasonal hydrology and probable impacts on floodplain forests. *Journal of Hydrology*, *349*, 397-410. doi: https://doi.org/10.1016/j.jhydrol.2007.11.012

A semi-distributed ntegrated itrogen model for multiple source assessment in tchments (INCA): Part I — model structure and process equations. (1998). *Science of The Total Environment*, *210-211*, 547–558. doi: 10.1016/S0048-9697(98)00037-0

Shi, X., Mao, J., Thornton, P. E., Hoffman, F. M., & Post, W. M. (2011). The impact of climate, co2, nitrogen deposition and land use change on simulated contemporary global river flow. *Geophysical Research Letters*, *38*. (https://doi.org/10.1029/2011GL046773) doi: https://doi.org/10.1029/2011GL046773

Sperotto, A., Molina, J. L., Torresan, S., Critto, A., Pulido-Velazquez, M., & Marcomini, A. (2019). A bayesian networks approach for the assessment of climate change impacts on nutrients loading. *Environmental Science & Policy*, *100*, 21-36. doi: https://doi.org/10.1016/j.envsci.2019.06.004

Streeter, H., & Phelps, E. (1925). *A study of the pollution and natural purification of the ohio river. iii. factors concerned in the phenomena of oxidation and reaeration.* U.S. Government Printing Office.

Suddick, E. C., Whitney, P., Townsend, A. R., & Davidson, E. A. (2013). The role of nitrogen in climate change and the impacts of nitrogen–climate interactions in the united states: foreword to thematic issue. *Biogeochemistry*, *114*, 1-10. doi: 10.1007/s10533-012-9795-z

Wexler, E. J. (1989). *Analytical solutions for one-, two-, and three-dimensional solute transport in ground-water systems with uniform flow* (Tech. Rep.). doi: 10.3133/ofr8956

Wexler, E. J. (1992). *Analytical solutions for one-, two-, and three-dimensional solute transport in ground-water systems with uniform flow*. US Government Printing Office.

Whitehead, P. G., Wilby, R. L., Battarbee, R. W., Kernan, M., & Wade, A. J. (2009). A review of the potential impacts of climate change on surface water quality. *Hydrological Sciences Journal*, *54*, 101-123. (doi: 10.1623/hysj.54.1.101) doi: 10.1623/hysj.54.1.101

Wilson, H., Elliott, J., Macrae, M., & Glenn, A. (2019). Near-surface soils as a source of phosphorus in snowmelt runoff from cropland. *Journal of Environmental Quality*, *48*, 921-930. doi: 10.2134/jeq2019.04.0155

Wilson, H. F., Casson, N. J., Glenn, A. J., Badiou, P., & Boychuk, L. (2019). Landscape controls on nutrient export during snowmelt and an extreme rainfall runoff event in northern agricultural watersheds. *Journal of Environmental Quality*, *48*, 841-849. doi: 10.2134/jeq2018.07.0278

Wood, E. F., Roundy, J. K., Troy, T. J., van Beek, L. P. H., Bierkens, M. F. P., Blyth, E., ... Whitehead, P. (2011). Hyperresolution global land surface modeling: Meeting a grand challenge for monitoring earth's terrestrial water. *Water Resources Research*, *47*(5). doi: https://doi.org/10.1029/2010WR010090

Wu, J., & Malmström, M. E. (2015). Nutrient loadings from urban catchments under climate change scenarios: Case studies in stockholm, sweden. *Science of The Total Environment*, *518-519*, 393-406. doi: https://doi.org/10.1016/j.scitotenv.2015.02.041

Wu, Y., Liu, S., & Gallant, A. L. (2012). Predicting impacts of increased co2 and climate change on the water cycle and water quality in the semiarid james river basin of the midwestern usa. *Science of The Total Environment*, *430*, 150-160. doi: https://doi.org/10.1016/j.scitotenv.2012.04.058

Yang, Q., Zhang, X., Almendinger, J. E., Huang, M., Chen, X., Leng, G., ... Li, X. (2019). Climate change will pose challenges to water quality management in the st. croix river basin. *Environmental Pollution*, *251*, 302-311. doi: https://doi.org/10.1016/j.envpol.2019.04.129

Ye, L., & Grimm, N. B. (2013). Modelling potential impacts of climate change on water and nitrate export from a mid-sized, semiarid watershed in the us southwest. *Climatic Change*, *120*, 419-431. doi: 10.1007/s10584-013-0827-z

Zheng, W., Wang, S., Tan, K., & Lei, Y. (2020). Nitrate accumulation and leaching potential is controlled by land-use and extreme precipitation in a headwater catchment in the north china plain. *Science of The Total Environment*, *707*, 136168. doi: https://doi.org/10.1016/j.scitotenv.2019.136168